CHAPTER 4

RESULTS AND DISCUSSION

4.1. Effective Number of Reflections in an IRE

4.1.1. ATR and Transmission Spectra

4.1.1.1. ATR Spectrum

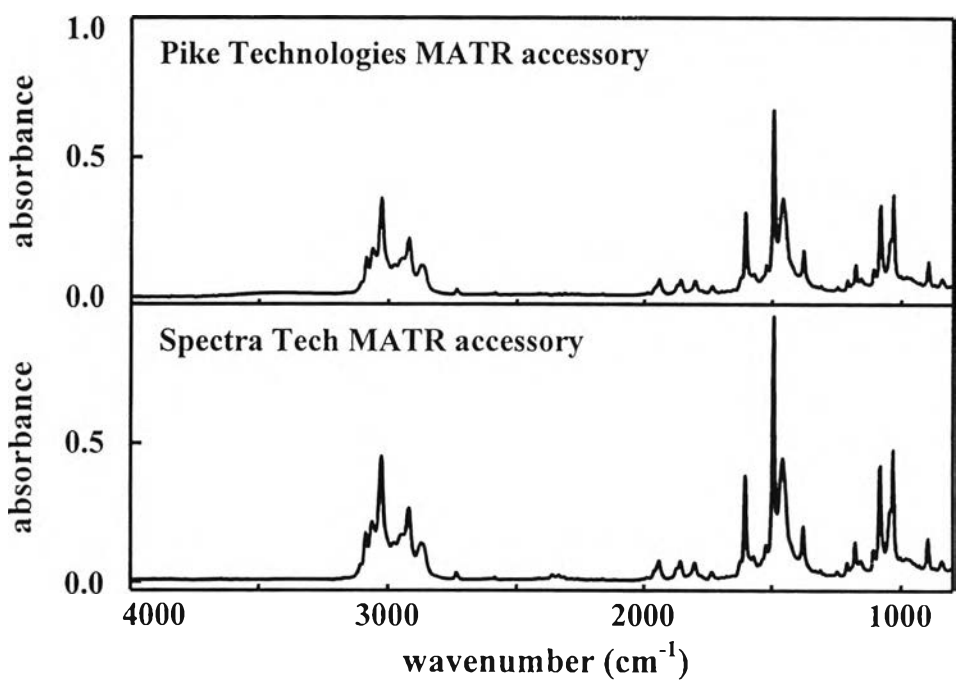

Figure 4.1 ATR spectra of toluene acquired by two commercially available MATR accessories using ZnSe IRE with 45° angle of incidence and non-polarized incident beam.

4.1.1.2. Transmission Spectrum

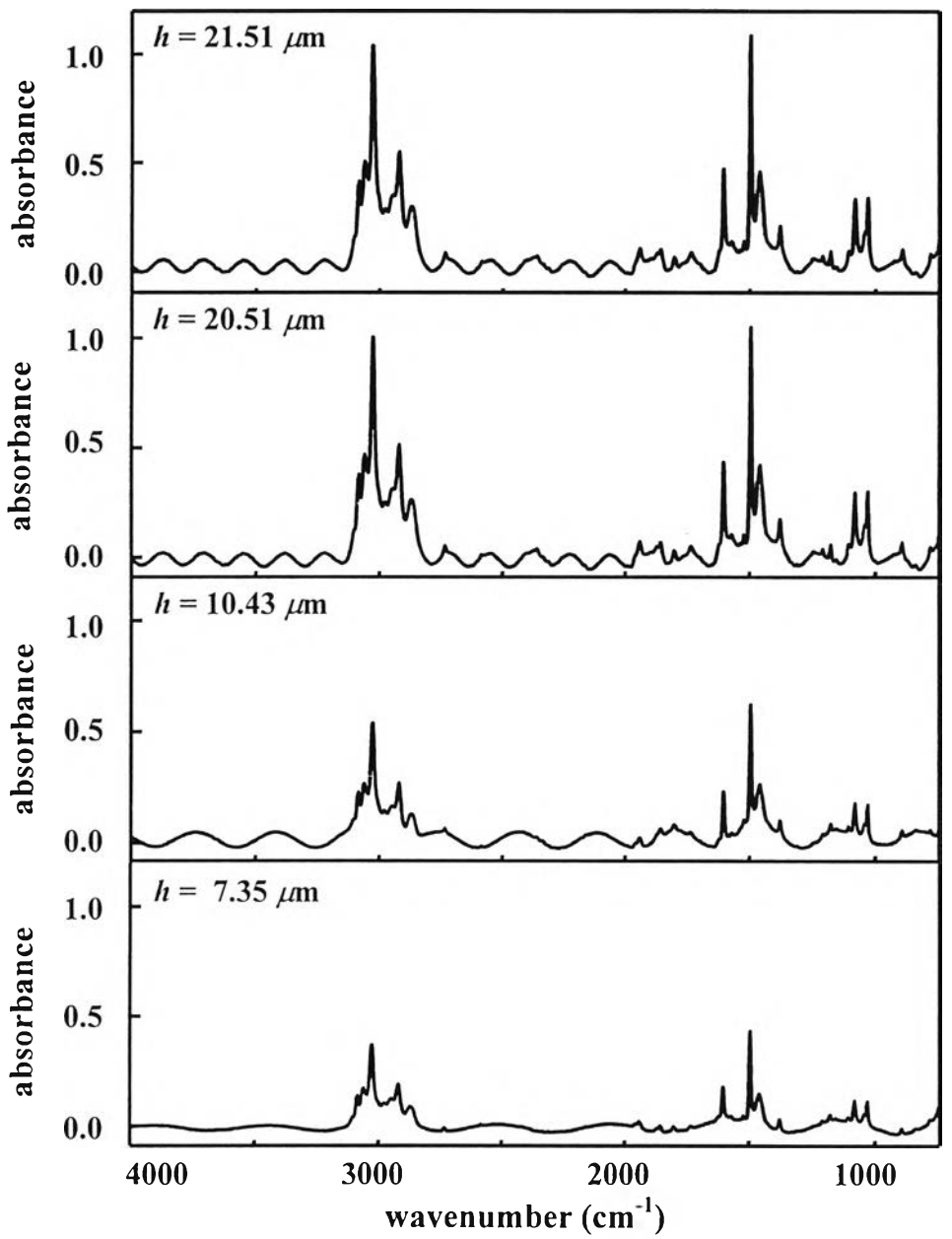

Figure 4.2 Transmission spectra of toluene collected via transmission cells with uniform thickness.

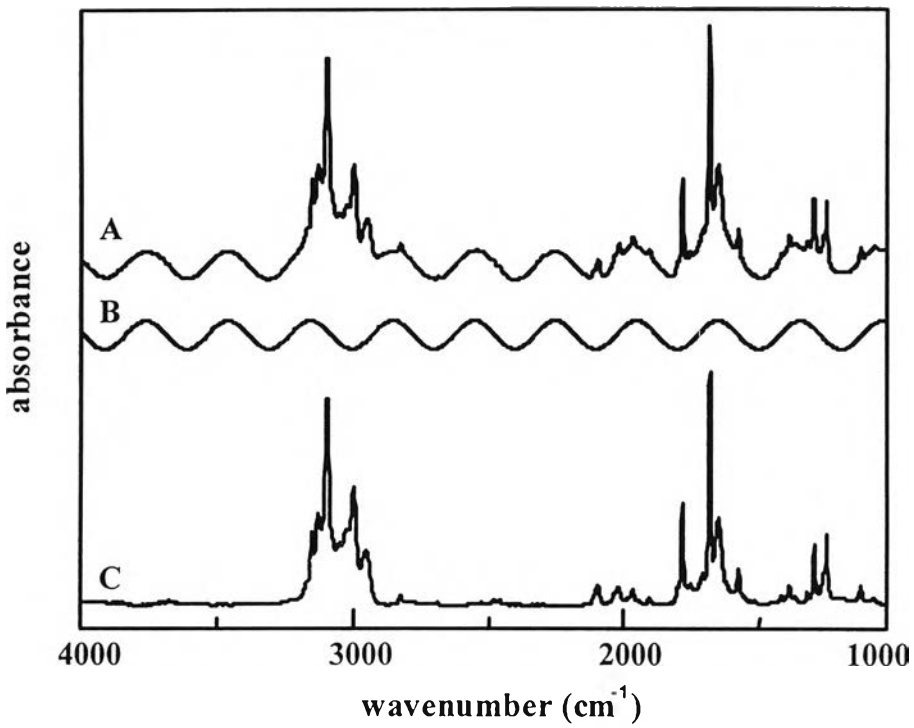

Figure 4.3 (A) transmission spectrum of toluene collected via transmission cell with uniform thickness, (B) simulated sinusoidal fringe spectrum, and (C) transmission spectrum of toluene after sinusoidal fringe subtraction.

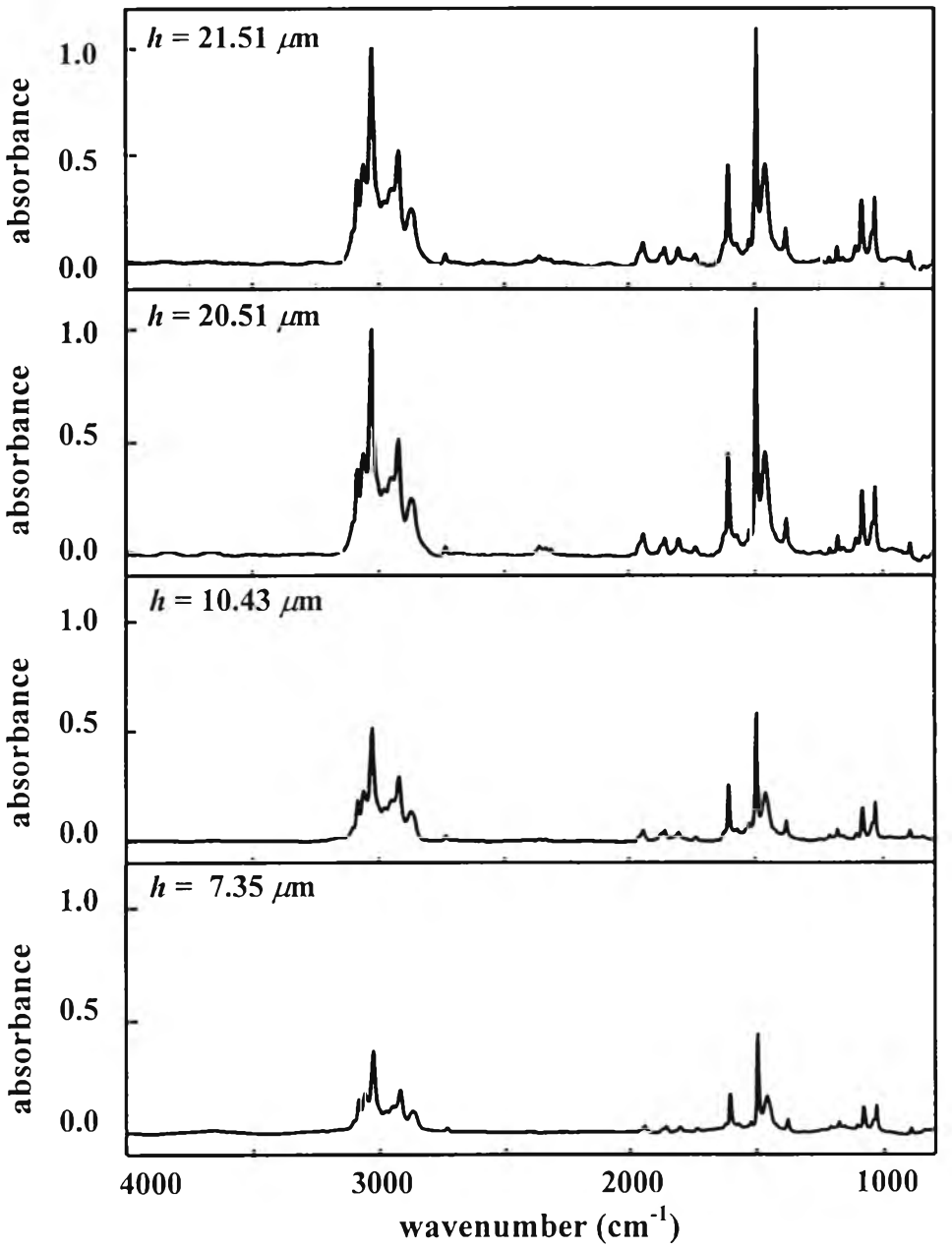

Figure 4.4 Transmission spectra of toluene shown in Figure 4.2 after interference fringe elimination via a mathematical mean.

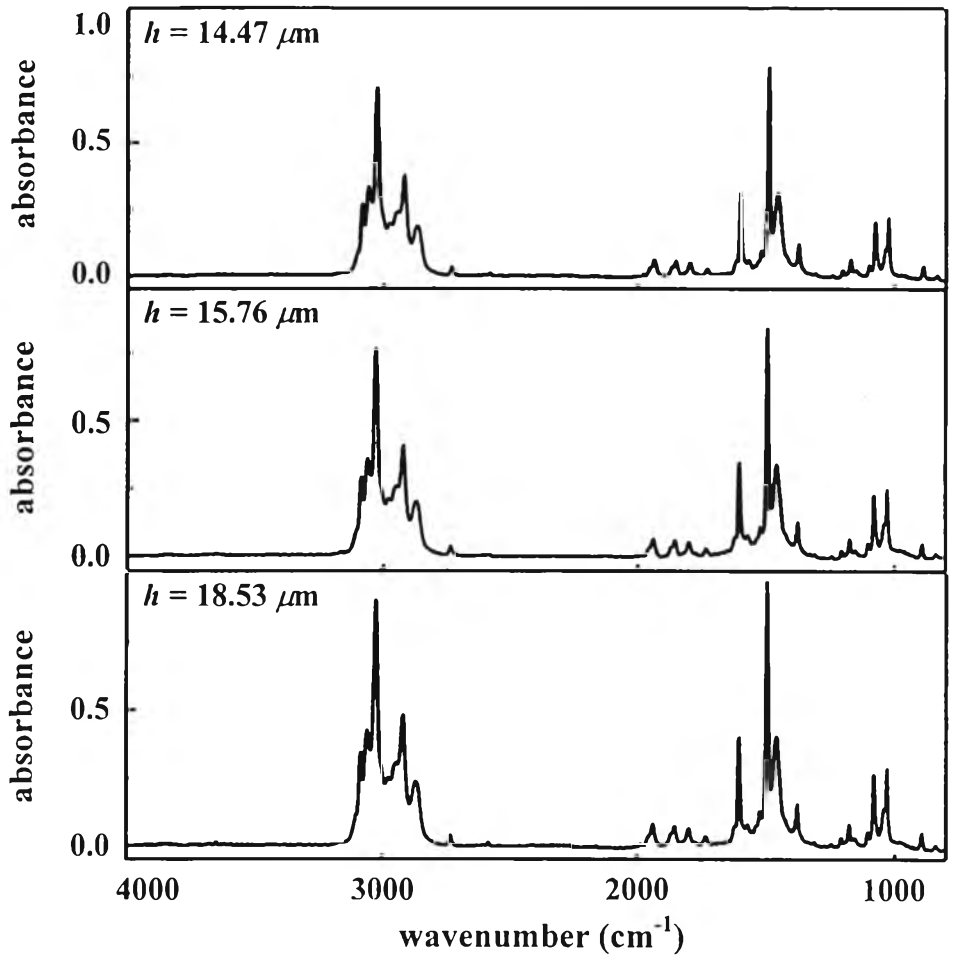

Figure 4.5 Transmission spectra of toluene collected via a wedge-shaped transmission cell. The average thickness of the cell is given in the figure.

4.1.2. Calibration Curves

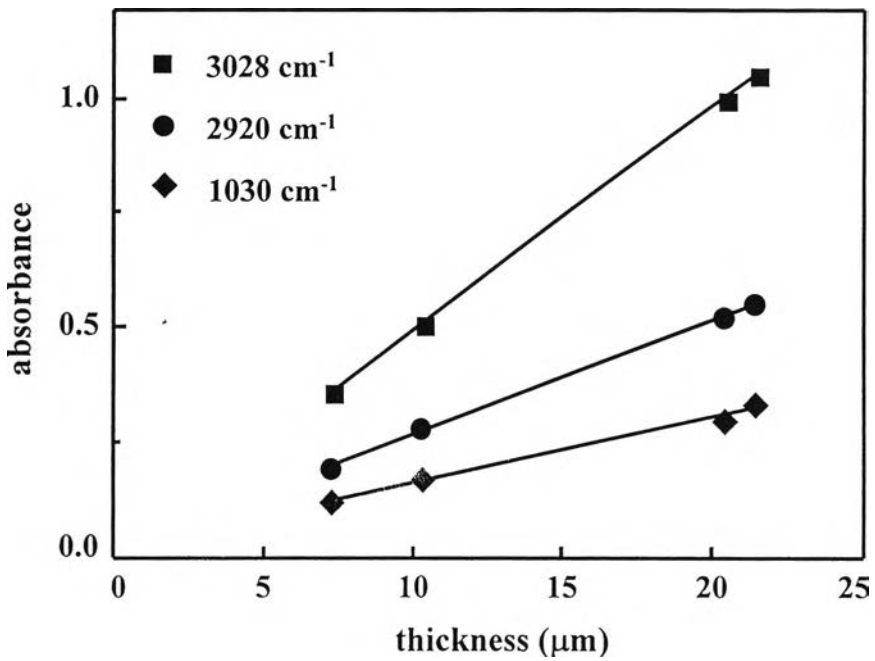

Figure 4.6 Calibration curves between thickness of transmission cell versus spectral intensity at various frequencies.

4.1.3. Calculated Value of Effective Number of Reflections

Table 4.1 Calculated effective number of reflections in 45° ZnSe IRE of MATR accessories using experimental results from transmission and ATR measurements.

wavenumber (cm^{-1})	Pike Technology Accessory[1]			Spectra Tech Accessory[2]		
	Thickness (μm)			Thickness (μm)		
	14.47	**15.76**	**18.53**	**14.47**	**15.76**	**18.53**
1030	5.63	5.57	5.64	7.49	7.42	7.51
1082	5.53	5.51	5.53	7.40	7.38	7.40
1379	6.28	6.39	6.39	7.79	7.93	7.92
1460	5.82	5.87	5.89	7.46	7.53	7.55
1605	5.51	5.51	5.62	7.12	7.12	7.25
2920	5.85	5.93	5.94	7.50	7.61	7.63
3028	5.43	5.51	5.54	7.07	7.16	7.21
$\bar{N}$	**5.72**	**5.76**	**5.79**	**7.40**	**7.45**	**7.50**
1495	4.65	4.73	4.88	6.69	6.80	7.01

[1] Theoretical N for the Pike Technology Accessory: 9.25.

[2] Theoretical N for the Spectra Tech Accessory: 10.00.

The ATR attachments being used in the entire experiment are multiple reflection attachment. According to Equation 2.17, ATR spectral intensity depends on both experimental parameters (i.e., degree of polarization, angle of incidence, and number of reflections in ATR prism) and material characteristics (i.e., refractive index of IRE and complex refractive index of the material). In order to perform quantitative analysis on an ATR spectrum (i.e., the relationship between spectral intensity and absorption index or concentration of the material), one must determine the accurate number of reflections in the IRE. The effective number of reflections in the IRE may not be the same as that obtained by the theoretical value (i.e., that from Equation 2.16) due to beam divergence and alignment of the attachment. There are two commercial MATR attachments being employed: Pike Technology MATR accessory and Spectra Tech MATR accessory. In order to eliminate the problem related to an optical contact between IRE and sample, a liquid sample: toluene, is utilized in this experiment. To calculate the effective number of reflections in an MATR accessory, spectra from transmission measurement and ATR measurement will be employed.

ATR Spectra of toluene acquired via the Pike Technology accessory and the Spectra Tech accessory are shown in Figure 4.1. Although the Pike Technology accessory is larger in physical dimension (i.e., 74x7x4 mm.) than the Spectra Tech accessory (i.e., 40x5x2 mm.) but its ATR spectral intensity is smaller than that obtained from the Spectra Tech accessory. This is due to the number of reflection in the Spectra Tech accessory is greater than that of the Pike Technology accessory. According to their physical dimensions and the angle of incidence, their theoretical number of reflections are 10.00 and 9.25 for the Spectra Tech and the Pike Technology accessories, respectively.

Figure 4.2 shows transmission spectra of toluene acquired by transmission cell with different thickness. The sinusoidal fringe patterns observed in the spectra are characteristic of multiple reflection between surface of film with uniform thickness. The sinusoidal fringe will not be found in spectra of films with non-uniform thickness, with rough surface or with wedge-shaped configuration. The

fringe is an undesirable feature in the spectrum since it interferes with quantitative characteristic of the spectrum. However, it can be employed for thickness calculation of the film. Once the fringe is eliminated, the spectra can be utilized for further quantitative calculation.

Due to insignificant refractive index dispersion in a non-absorbing region (i.e., 3000 – 4000 cm^{-1}), the sinusoidal fringe pattern in this region was employed for the calculation of transmission cell thickness. In order to preserve the quantitative relationship between spectral intensity and sample thickness, the elimination of the sinusoidal fringes by a mathematical mean was employed (see Figure 4.3). The calculated cell thickness was used to simulate the sinusoidal fringe spectrum over the mid-infrared region via the optical theory (a constant refractive index of 1.47 is assumed [11, 14]). The sinusoidal fringes in a transmission spectra shown in Figure 4.2 were then eliminated by using spectral subtraction. The observed spectrum with sinusoidal fringe, the fringe calculated by optical theory, and the obtained spectra after fringe elimination are shown in Figure 4.3. The fringe-eliminated spectra were then used for the construction of calibration curves between the spectral intensity and thickness of transmission cell. This calibration curves are shown in Figure 4.6. The curves were later used for thickness determination of the wedge-shaped transmission cell from which the observed spectra without sinusoidal fringes were acquired.

Interference fringe-free transmission spectra are shown in Figure 4.5. These spectra were collected using a wedge-shaped sandwich cell. The thickness of the cell was calculated from the calibration curves at various frequencies. The average thickness was then used to calculate the effective number of reflections. In order to suppress the error associated to an individual spectrum, the thickness from calibration curves and spectral intensity from a wedge-shaped transmission cell were employed instead of those from interference fringe spectra. According to Figure 4.4, one would quickly notice residual fringes in the spectra since there is no mathematical mean for complete elimination of the interference fringe due to refractive index dispersion around the absorption bands.

The effective numbers of reflections of both commercial MATR attachments were calculated from the observed ATR and transmission spectra. The results are shown in Table 4.1. The values calculated from experimental data are always smaller than the theoretical values. In comparison to the Spectra Tech accessory, the Pike Technologies accessory has smaller number of reflections relative to the theoretical value. Since the Pike Technology IRE is bigger, the incident beam travels with a greater distance in the IRE. As a result, the effect of the beam divergence is more pronounced. Excluding the values obtained by the spectral intensities at 1495 cm^{-1}, the average effective numbers of reflections are 5.76 (SD = 0.30) and 7.45 (SD = 0.25) for accessories from Pike Technologies and Spectra Tech, respectively. The variation in the calculated values is due to refractive index dispersion and noise in the spectra. The refractive index dispersion is more pronounced around strong absorption bands compared to weak absorption bands. At 1495 cm^{-1}, the effective number of reflections is slightly smaller than at other frequencies. This is due to a non-linear relationship between the spectral intensity and absorption coefficient at that frequency [10, 14]. All spectral intensities employed for the calculation must be within linear relationship region between spectral intensity and absorption coefficient.

4.2. Optical Contact in ATR Experiment

4.2.1. ATR Spectrum

4.2.1.1. ZnSe/*i*-propanol/PVC System

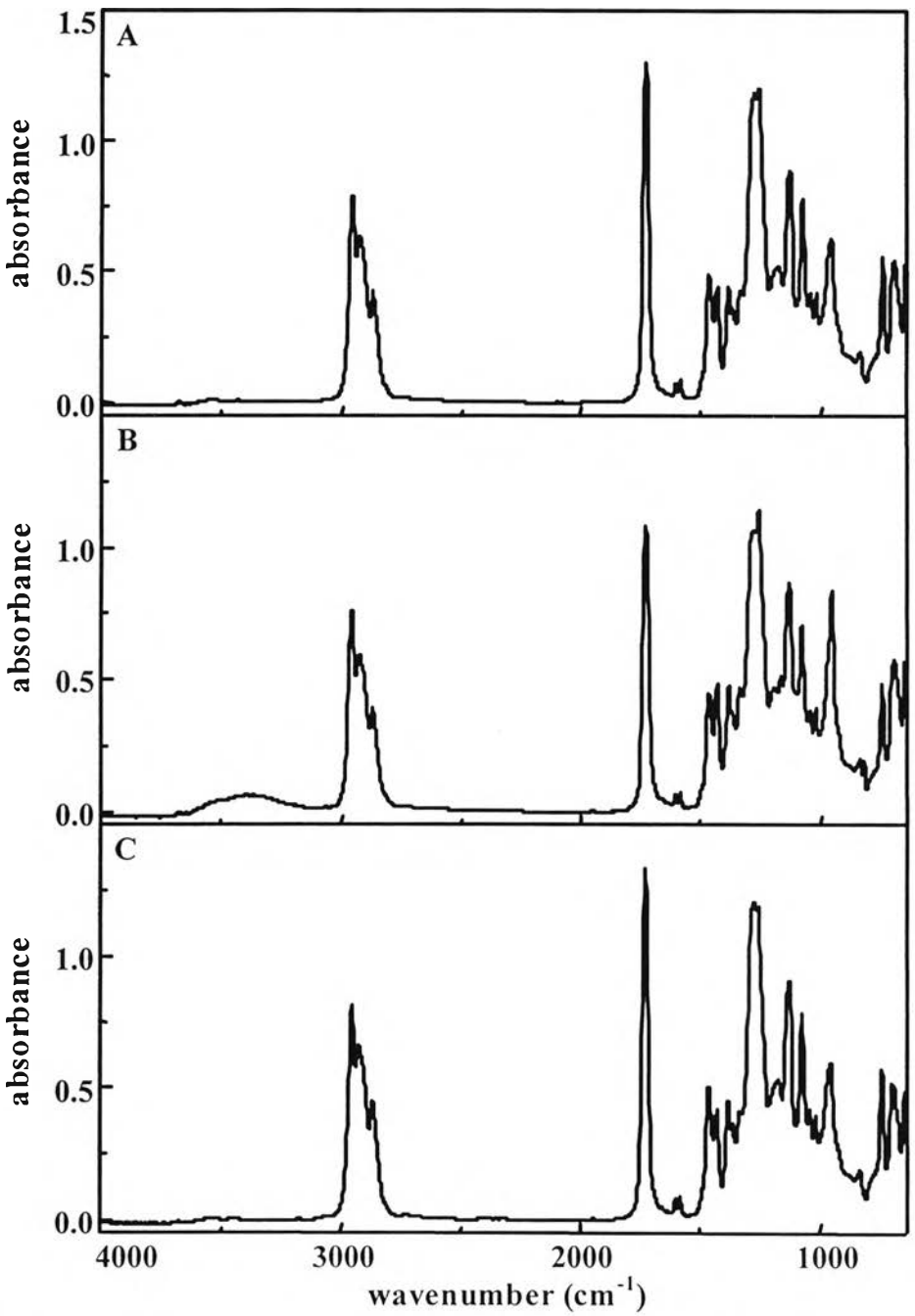

Figure 4.7 ATR spectra of *i*-propanol/PVC system acquired via 45° ZnSe IRE; spectrum of PVC on IRE (A), spectrum of PVC with *i*-propanol layer (B), and spectra of (B) after *i*-propanol was completely removed.

4.2.1.2. ZnSe/ *i*-propanol/PC System

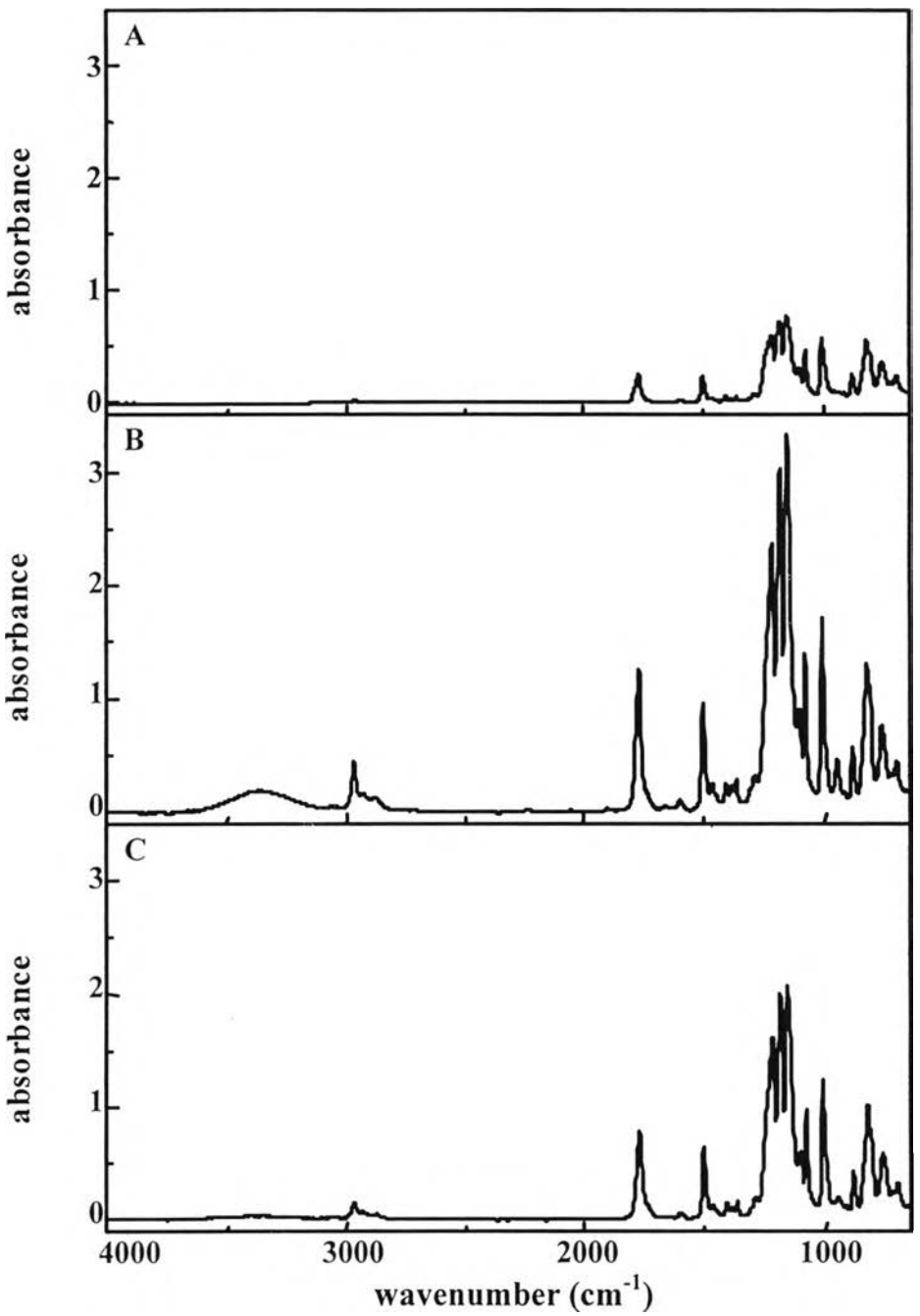

Figure 4.8 ATR spectra of *i*-propanol/PC system acquired via 45° ZnSe IRE; spectrum of PC on IRE (A), spectrum of PC with *i*-propanol layer (B), and spectra of (B) after *i*-propanol was completely removed.

4.2.1.3. ZnSe/Nujol/PVC System

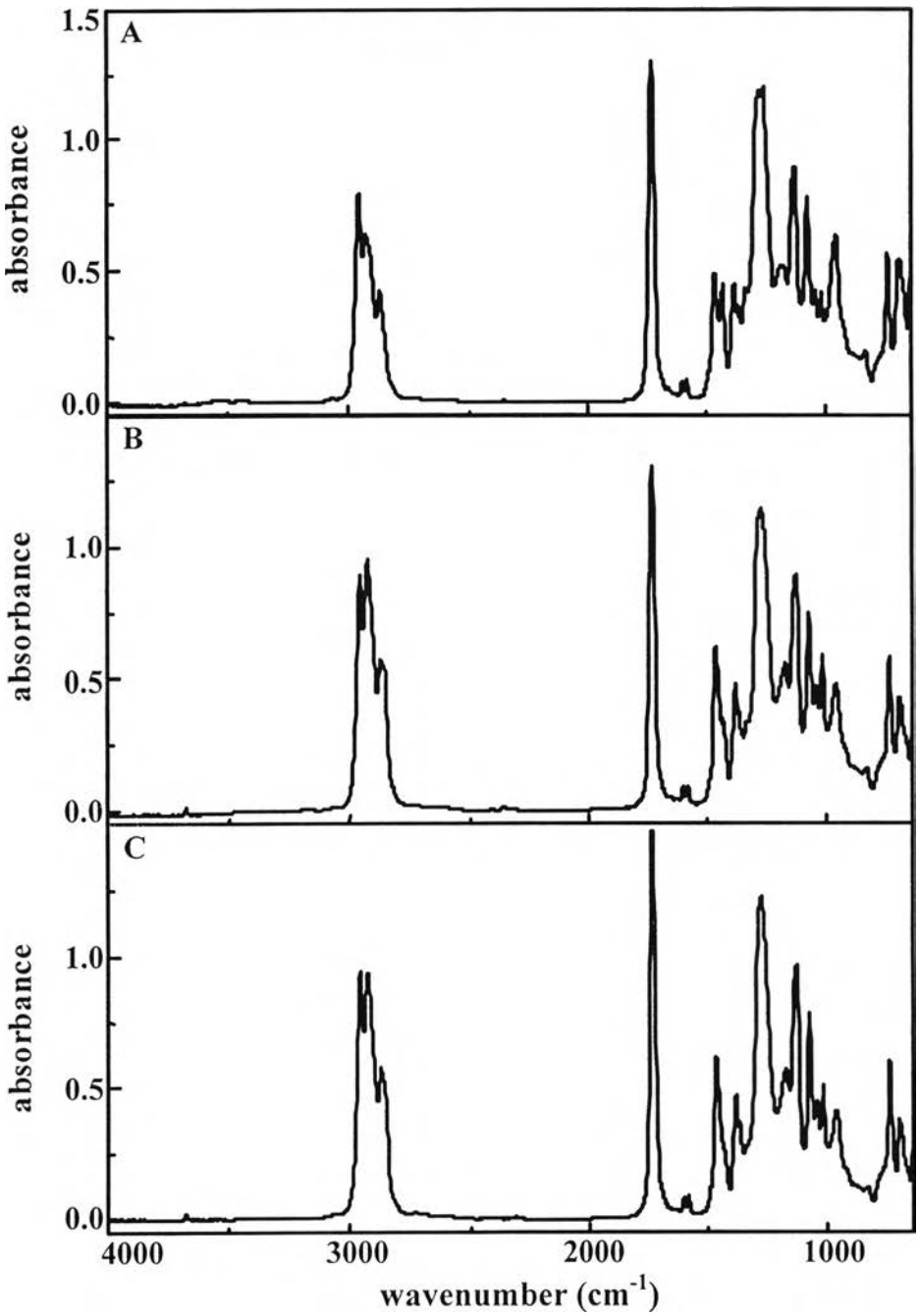

Figure 4.9 ATR spectra of Nujol/PVC system acquired via 45° ZnSe IRE; spectrum of PVC on IRE (A), spectrum of PVC with Nujol layer (B), and spectra of (B) after Nujol was completely removed.

4.2.1.4. ZnSe/Nujol/PC System

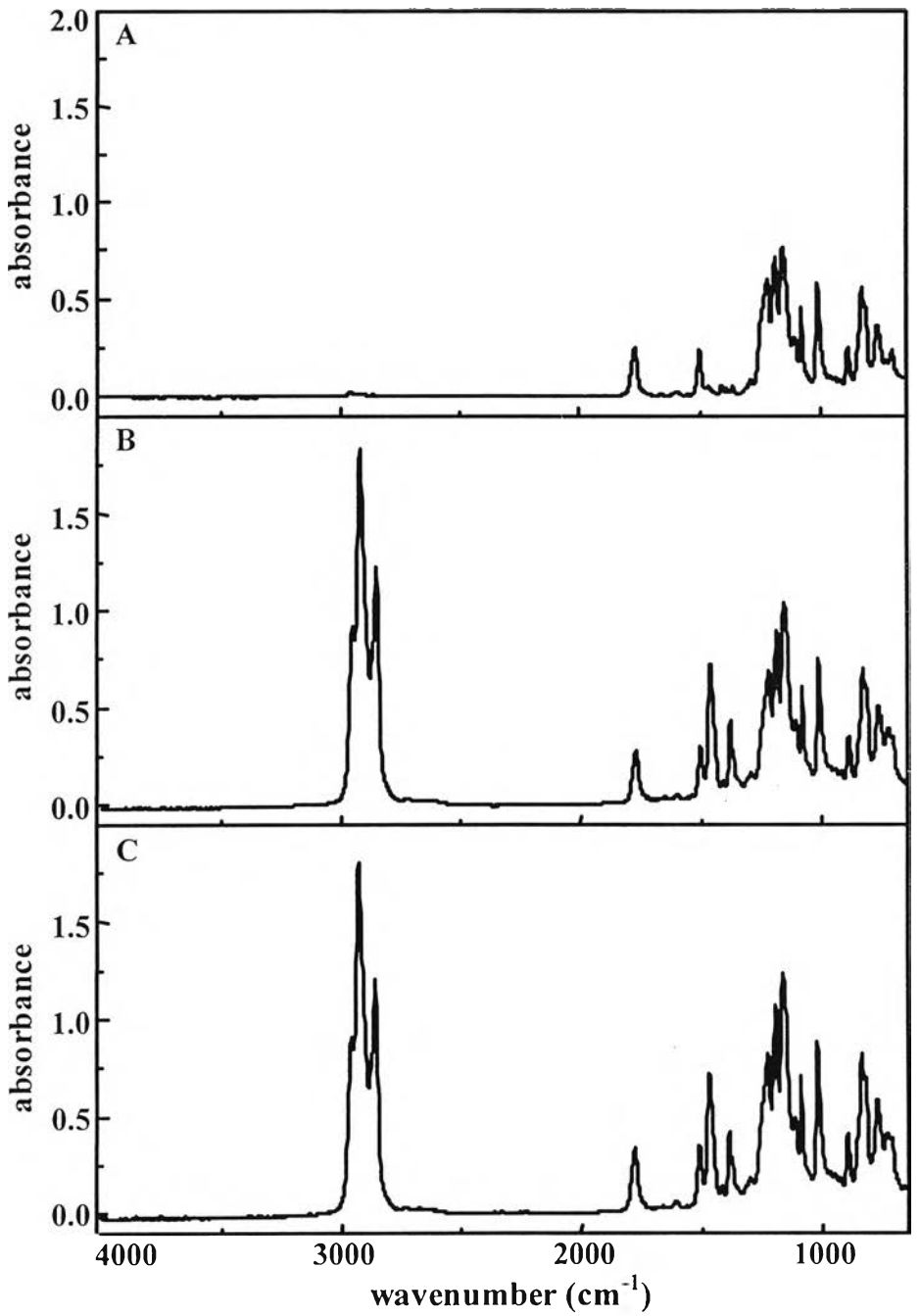

Figure 4.10 ATR spectra of Nujol/PC system acquired via 45° ZnSe IRE; spectrum of PC on IRE (A), spectrum of PC with Nujol layer (B), and spectra of (B) after Nujol was removed.

4.2.1.5. Ge/*i*-propanol/PVC System

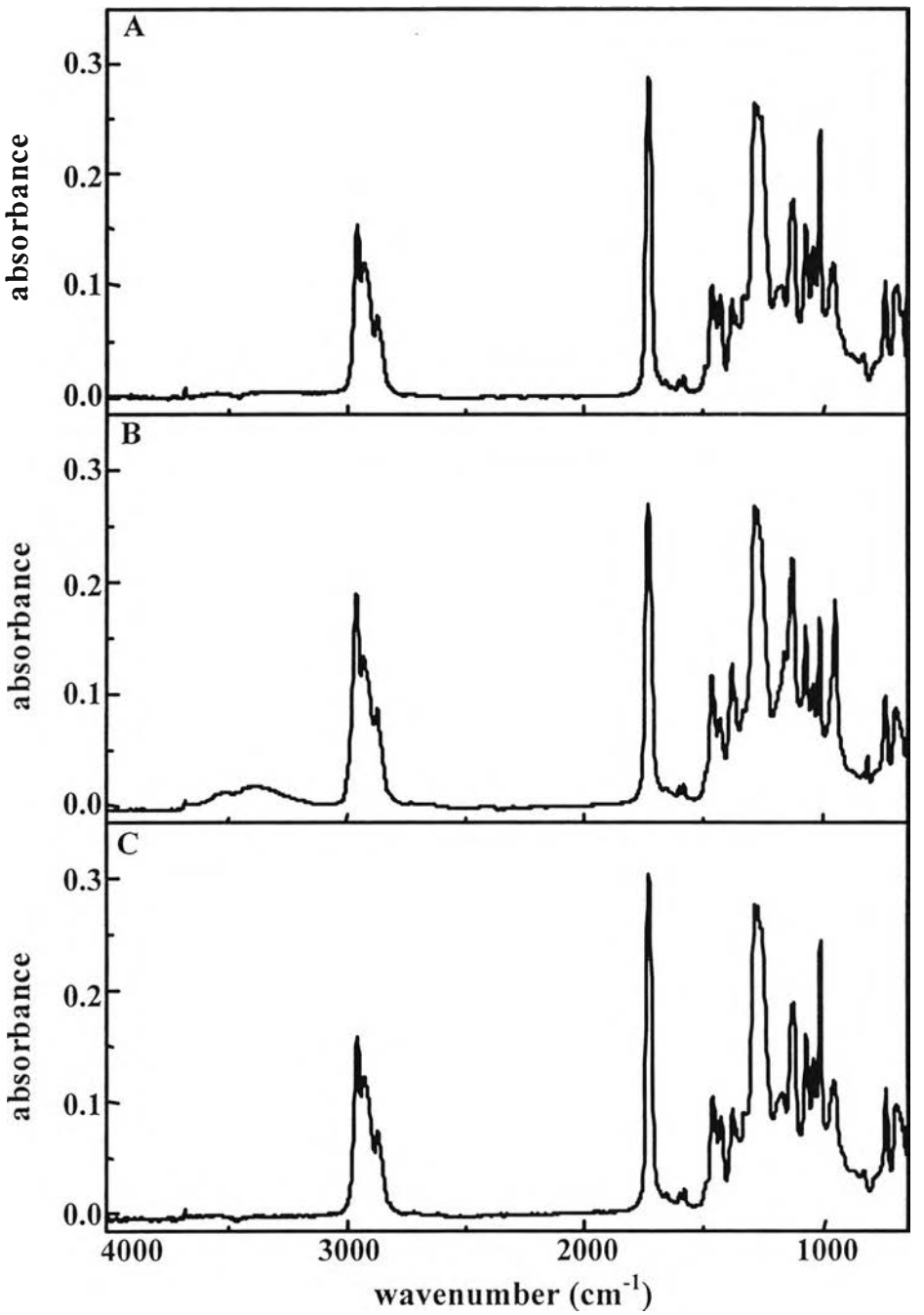

Figure 4.11 ATR spectra of *i*-propanol/PVC system acquired via 45° Ge IRE; spectrum of PVC on IRE (A), spectrum of PVC with *i*-propanol layer (B), and spectra of (B) after *i*-propanol was completely removed.

4.2.1.6. Ge/*i*-propanol/PC System

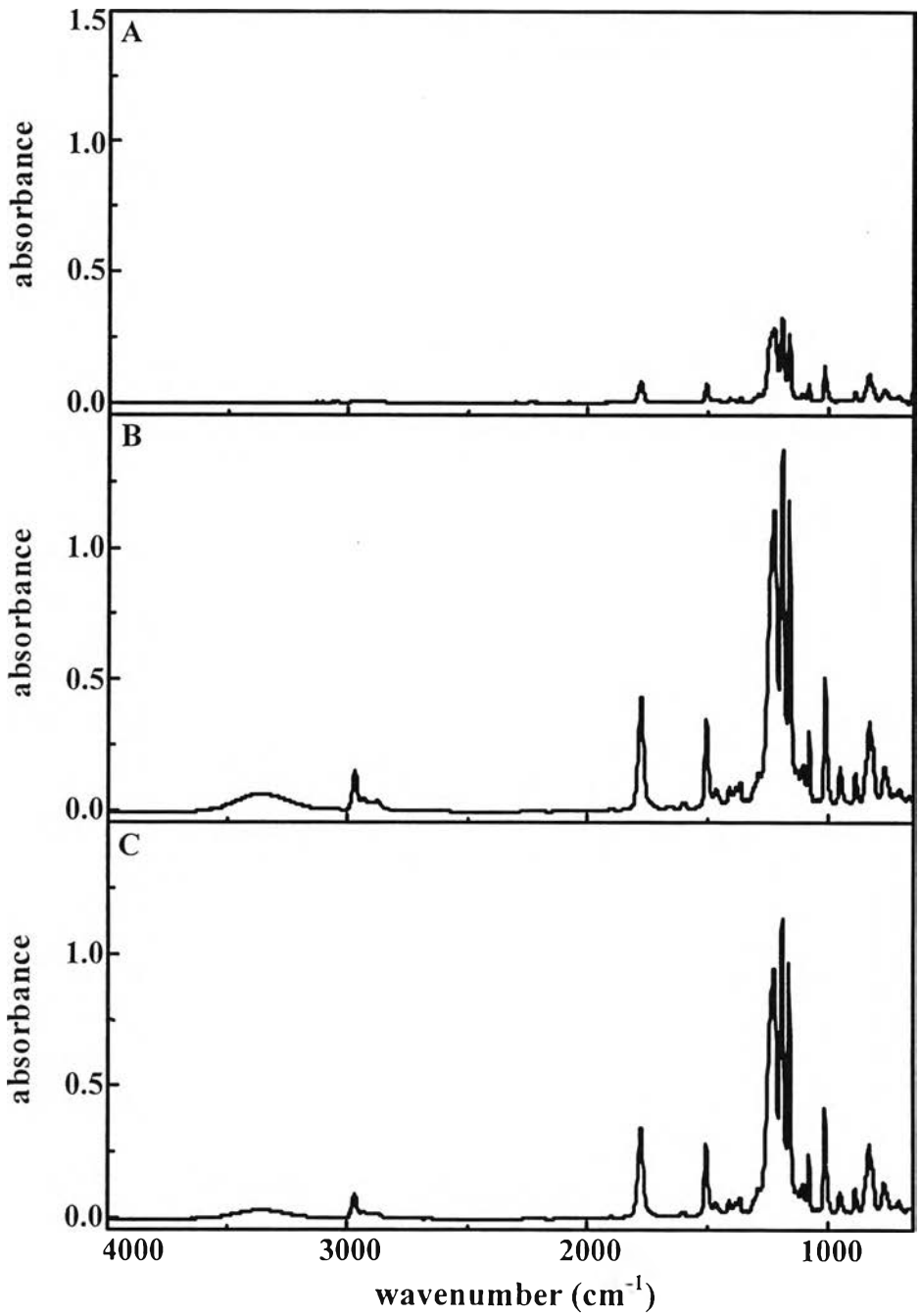

Figure 4.12 ATR spectra of *i*-propanol/PC system acquired via 45° Ge IRE; spectrum of PC on IRE (A), spectrum of PC with *i*-propanol layer (B), and spectra of (B) after *i*-propanol was completely removed.

4.2.1.7. Ge/Nujol/PVC System

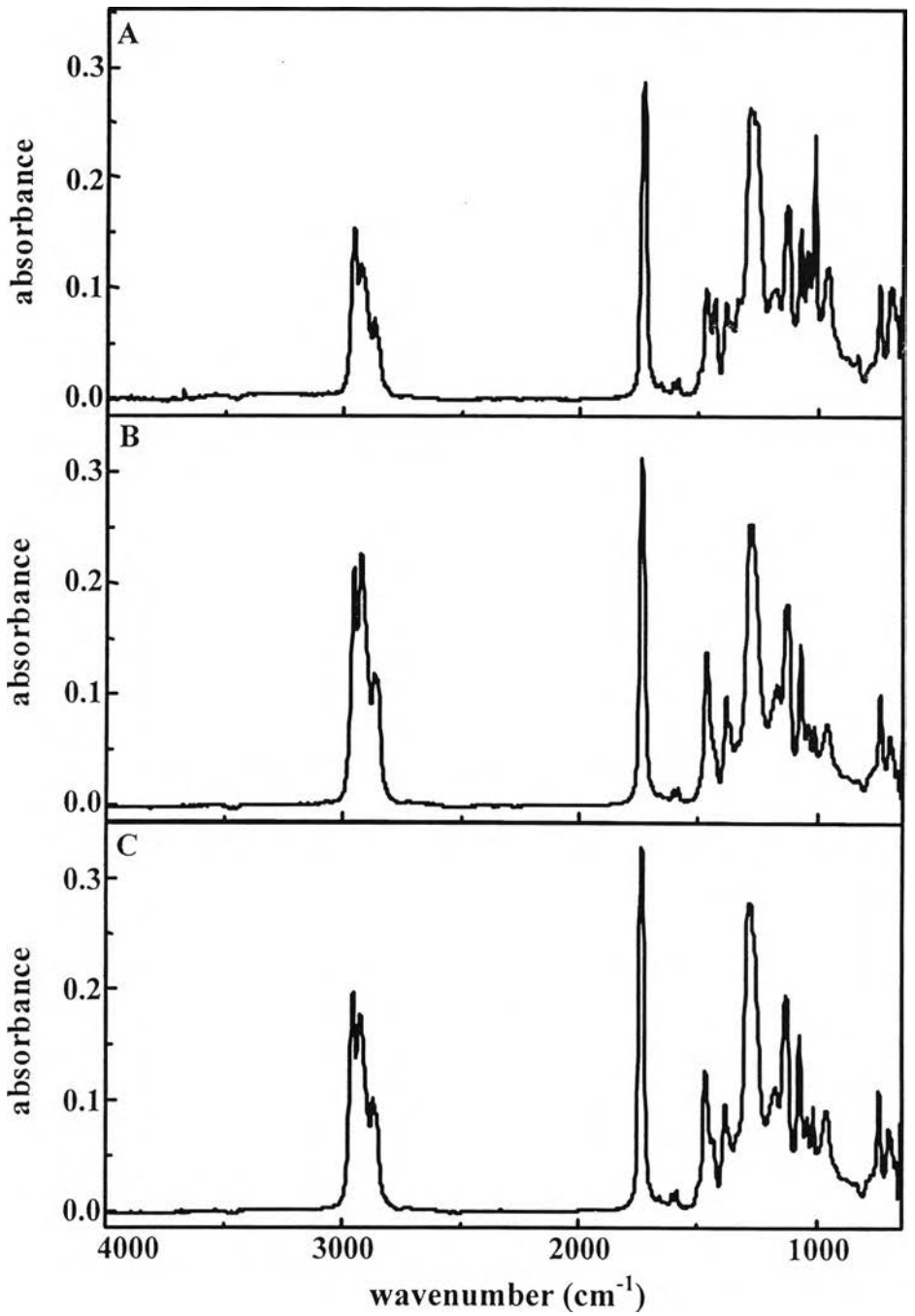

Figure 4.13 ATR spectra of Nujol/PVC system acquired via 45° Ge IRE; spectrum of PVC on IRE (A), spectrum of PVC with Nujol layer (B), and spectra of (B) after Nujol was completely removed.

4.2.1.8. Ge/Nujol/PC System

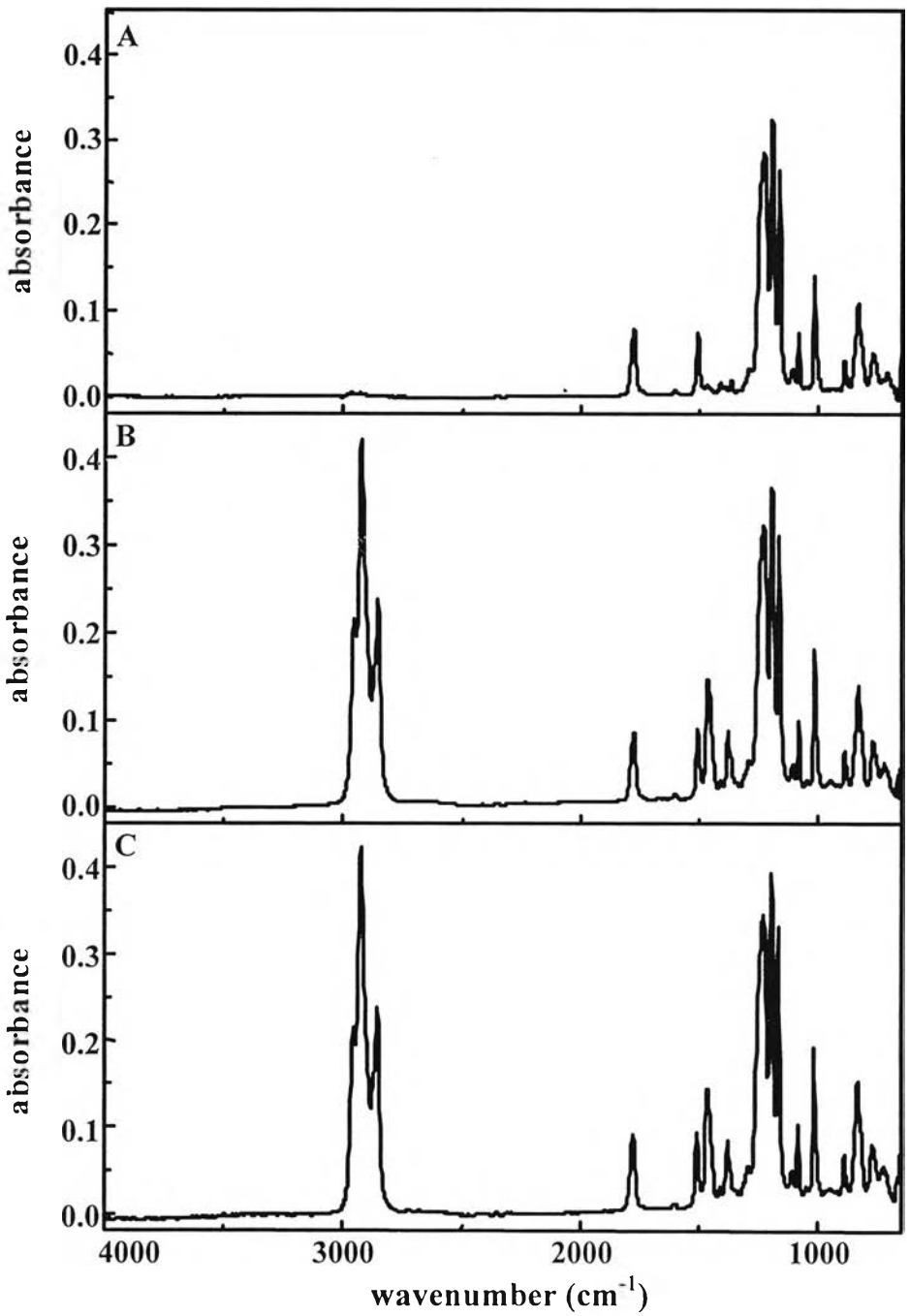

Figure 4.14 ATR spectra of Nujol/PC system acquired via 45° Ge IRE; spectrum of PC on IRE (A), spectrum of PC with Nujol layer (B), and spectra of (B) after Nujol was removed.

According to Equation 2.17, a perfect contact or optical contact between IRE and sample is assumed. The optical contact requirement must be satisfied in order to apply Equation 2.17 for further analysis. Furthermore, the decay characteristic of the MSEF is drastically changed when an air gap presents in the system (see Figure 2.10). Therefore, it is necessary to verify whether the system under investigation has an optical contact or not. A technique for optical contact verification and a technique for improving optical contact will be proposed.

Figure 4.7 shows ATR spectrum of ZnSe/*i*-propanol/PVC system. Spectrum A is ATR spectrum of PVC sample placed into contact with ZnSe IRE by an applied pressure. The spectrum was acquired without any intermediate layer. PVC sample was pressed against the IRE so close that any air gap could not be seen when viewed through the sample from the top. Since PVC is flexible, it makes a good contact with the surface of the IRE. Spectrum B is ATR spectrum of a three-phase system of ZnSe/*i*-propanol/PVC. Pressure was applied to the PVC in order to squeeze the *i*-propanol out. Spectrum B was acquired when there is thin *i*-propanol film left in the system. The pressure was applied until the *i*-propanol was completely removed, spectrum C was, then, acquired. Spectrum C indicates that there is no *i*-propanol left in the system since there is no characteristic band of *i*-propanol in the spectrum. From spectrum A and spectrum C, one will quickly notice that their spectral intensities is not so much different (those of C are slightly greater than those of A). This implies that the contact between IRE and PVC is not greatly improved in the liquid-assisted system (i.e., IRE/*i*-propanol/PVC). Since PVC is flexible, its flat surface can easily make a good contact with the IRE. As a result, the contact cannot be improved further.

ATR spectrum of ZnSe/*i*-propanol/PC system are shown in Figure 4.8. Unlike PVC sample, PC sample is a glass-like polymer. A good contact is difficult to obtain. Although its surface is obviously flat, a contact between PC and IRE is poor. ATR spectrum of PVC without any assistance for contact improvement beside the applied pressure is shown in spectrum A. When *i*-propanol was introduced between the PC sample and the IRE (see spectrum B) the spectral intensity of PC sample is

drastically enhanced. This is due to the air gap was replaced by *i*-propanol. The refractive index of *i*-propanol (i.e., $n_{i\text{-propanol}} = 1.5$) is higher than that of air (i.e., $n_{air} = 1.0$). The electric field at the interface region decays slower in the *i*-propanol and penetrates deeper into the sample compared to the system with air gap. Furthermore, the refractive index of *i*-propanol is not so much different from that of the PC sample, the decay patterns of the MSEF in both samples are not so much different. Moreover, both the applied pressure and the evaporation of *i*-propanol induce capillary force to pull the two surfaces coming closer. However, it should be noted that as *i*-propanol was completely evaporated (see spectrum C), without any change in the applied pressure, the spectral intensity of PC sample is decreased (i.e., smaller than spectrum B) but stills greater than that of spectrum A. According to this, it can be concluded that there is still no optical contact in the system or there is still a gap between the PC and the IRE surfaces.

Figure 4.9 shows ATR spectrum of ZnSe/Nujol/PVC system. As mentioned before, PVC can make a good contact with the IRE and air gap rarely exists. According to spectra A, B, and C, a perfect contact between PVC and the IRE cannot be achieved by simply apply pressure on the polymer (i.e., spectrum A). Spectral intensity is increased when a thin film of Nujol is introduced in the system. This indicates that the contact between sample and IRE can be improved by thin organic film. When Nujol was completely squeezed out of the system, a better contact is achieved (i.e., spectrum C). Spectral intensity of PVC is significantly increased when compared to that of the un-assisted system.

Figure 4.10 shows ATR spectrum of ZnSe/Nujol/PC system. Like other systems, the spectral intensity of PC sample is enhanced when Nujol was introduced (see spectrum A, B, and C.) However, an optical contact between PC and IRE cannot be achieved. Spectrum C indicates that Nujol cannot be completely removed from the system. This is due to the glassy-like nature of PC. Although the surface of PC sample is flat but the long-range unevenness make the surface contact between IRE and sample poor. As a result, Nujol cannot be removed by simply applying pressure to the system. However, spectral enhancement is observed when Nujol presents in

the system. This is due to the decay characteristic of the MSEF in air gap-present and Nujol-present systems. The decay pattern of the MSEF in the latter case is similar to that in polymer-only system with perfect optical contact. But still the optical contact between PC sample and the IRE was not obtained since Nujol cannot be completely eliminated from the system as can be seen in spectrum B and spectrum C.

Shown in Figure 4.11 are ATR spectra of Ge/*i*-propanol/PVC system. Similar results as in case of ZnSe IRE were observed but the spectral intensity, which is smaller than that in case of ZnSe IRE. This is due to Ge has higher refractive index than ZnSe. The electric field in the system using Ge as an IRE decays faster than that using ZnSe as an IRE. As a result, the penetration is smaller in the case of Ge. Due to a large difference between Ge and sample, the field strength in the Ge system is smaller than that in the ZnSe system. As a result of the above influences, field strength and field decay, spectral intensity of a material with Ge as an IRE is smaller than that with ZnSe as an IRE. Spectra A and C indicate that PVC and IRE already have a good contact since PVC is flat and flexible. Surface contact improvement by introduction of liquid film does not significantly improve the existing contact.

ATR spectra of Ge/*i*-propanol/PC system are shown in Figure 4.12. In case of PC sample, like ZnSe/*i*-propanol/PC system, the spectral intensity of PC sample is drastically increased when *i*-propanol was introduced between the sample and the IRE. The intensity is slightly decreased when *i*-propanol was completely eliminated. The influence of liquid-assist contact improvement is more pronounced when Ge is employed as an IRE. This is due to the decay characteristic of the electric field in the system. The electric field with Ge as an IRE decay very fast as a function of depth compared to that with ZnSe as an IRE (see Figure 2.6). As a result, a small air gap drastically decreases spectral intensity (as in Figure 4.12 A). When the air gap was decreased in thickness, the intensity is significantly increased since a portion of electric field with greater strength can interact with the sample (Figure 4.11 C). However, if the same air gap is filled with organic liquid with refractive index similar to that of the sample, the intensity is further increased. The decay pattern of the electric field is altered since the refractive index mismatch is eliminated.

Figure 4.13 shows ATR spectra of Ge/Nujol/PVC system. Spectral intensity of PVC sample is increased when Nujol presents. The same effect was also observed when Nujol was eliminated. However, the spectral enhancement with Ge as an IRE is more pronounced compared to system with ZnSe as an IRE. This is due to the decay characteristic of the electric field. The field decays rapidly to an insignificant level within a short distance where Ge is employed as an IRE (see Figure 2.6). As a result, a better contact will drastically improve the spectral intensity since the portion of electric field with a greater strength (i.e., those near the surface of IRE) can interact with the material.

ATR spectra of Ge/Nujol/PC system are shown in Figure 4.14. The spectral intensity of PC sample is enhanced by Nujol but not as much as in case of *i*-propanol. This is because Nujol cannot be completely removed. Therefore, the ability in pulling the two surfaces to become closer is much less than that of *i*-propanol.

From experimental results, it was found that an optical contact between solid samples and the IRE is crucial for further analysis and application of the observed spectrum. However, it cannot be easily achieved by simply applying pressure to the system. Different types of samples (i.e., flexible and rigid samples) show different degree of contact to the IRE surface. Although the surface of the sample seen to be flat, the lack of long-range uniformity makes a good contact becomes difficult to achieve. The contact improvement is required in order to acquire bulk spectral intensity of the sample for further analysis. The liquid film is introduced into the system in order to improve the contact. Easily evaporated liquid (i.e., *i*-propanol) seems to improve the contact significantly. The less volatile liquid (i.e., Nujol), on the other hand, improve contact of flexible polymer since the liquid can be squeezed out by the applied pressure.

In order to determine the sampling depth in ATR FT-IR spectroscopy, according to Equation 2.21, the bulk spectral intensity of sample is required. Therefore, the spectral intensity of ATR spectrum of both solid samples (i.e., PVC sample and PC sample) will not be employed for the calculation of sampling depth

via the proposed equation. Since a perfect contact or optical contact cannot be achieved. ATR spectrum of liquid sample (i.e., Nujol and *i*-propanol) will be used instead of that of the solid sample. This approach is valid since the refractive indices of all organic materials are almost the same. Furthermore, the contact problem is eliminated.

4.3. Sampling Depth in ATR FT-IR Spectroscopy

4.3.1. ATR Spectra of ZnSe/Nujol/PVC System

4.3.1.1. Two-Phase System Spectrum

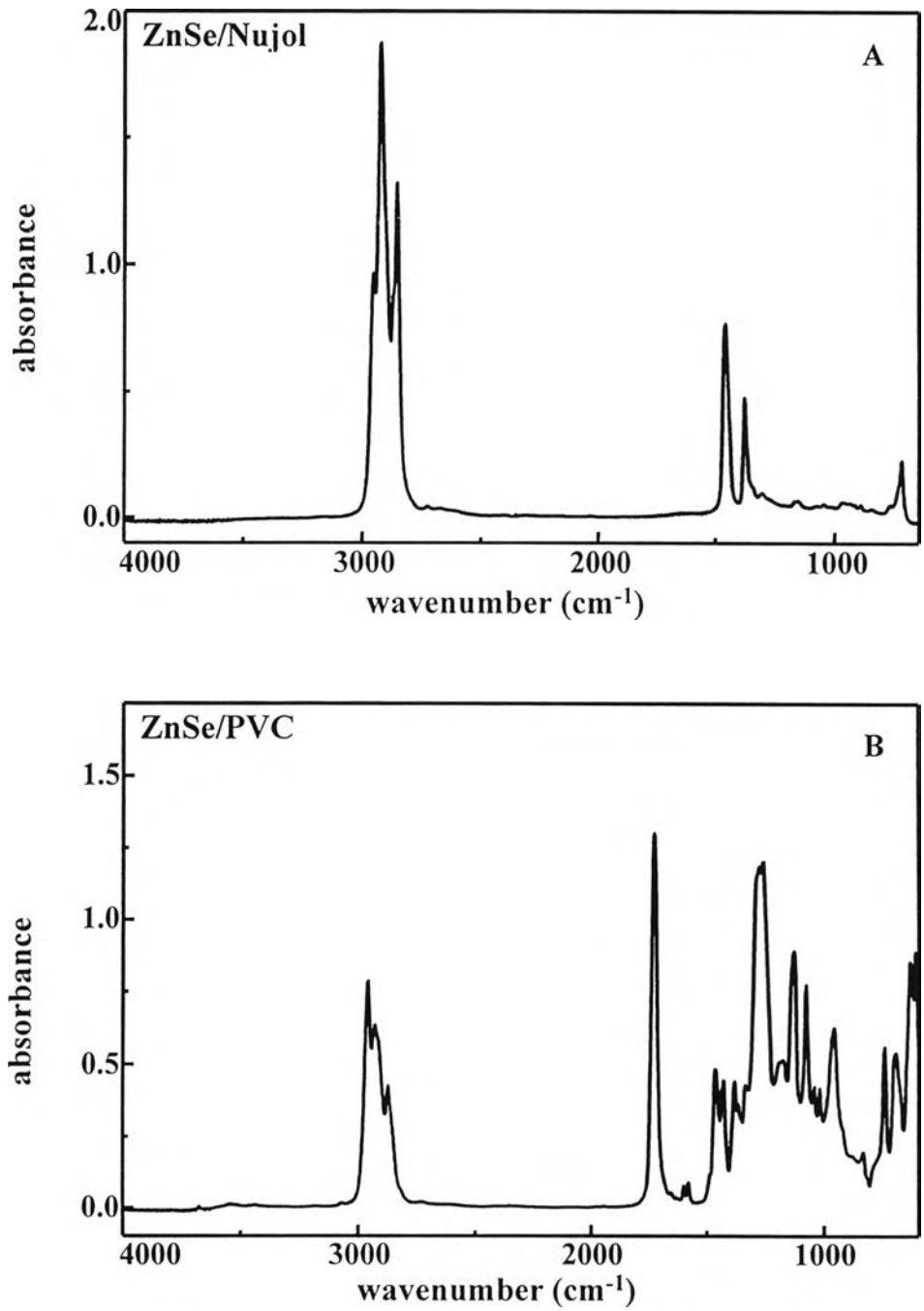

Figure 4.15 ATR spectrum of Nujol and PVC acquired via 45° ZnSe IRE.

4.3.1.2. Three-Phase System Spectrum

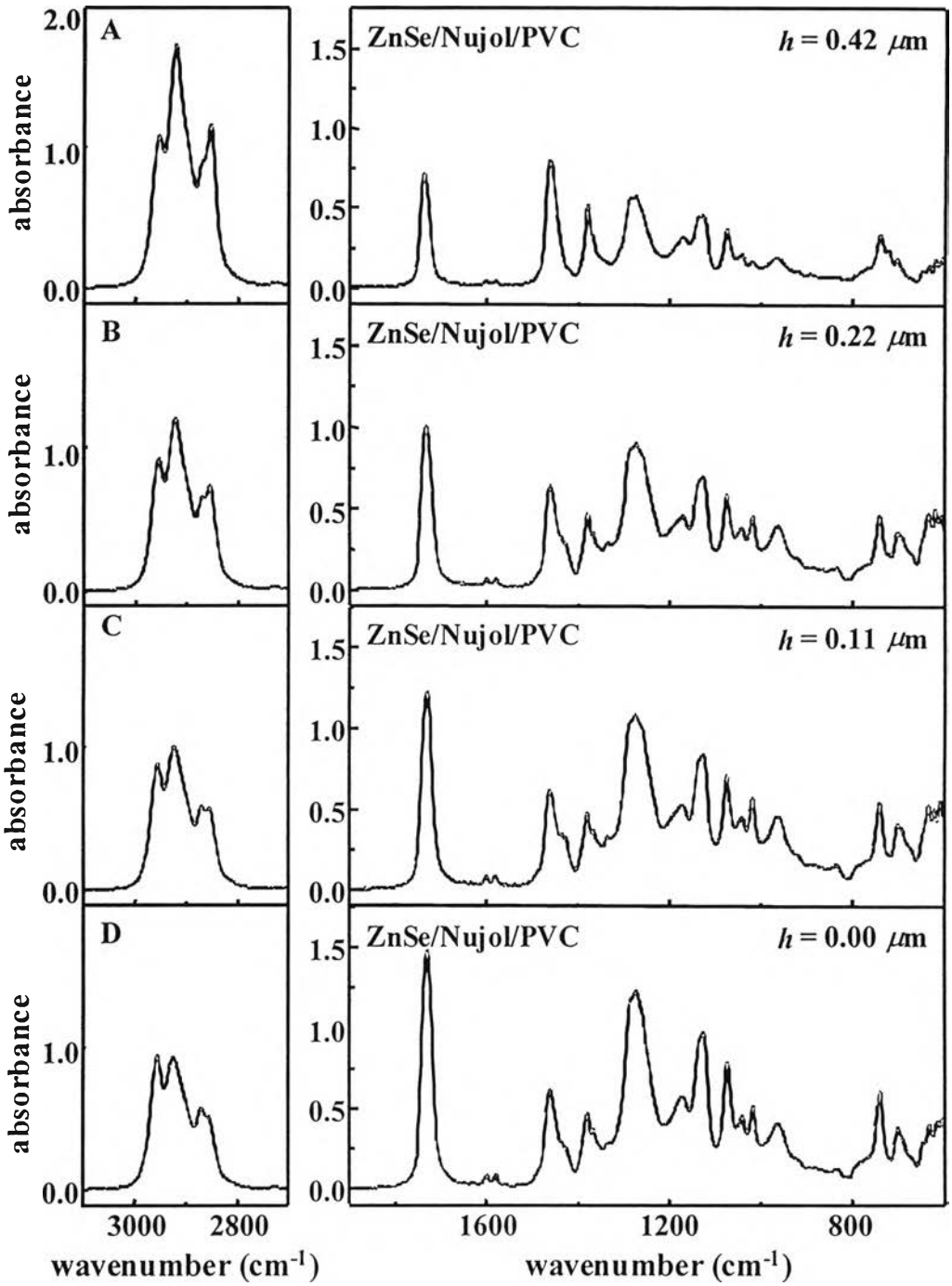

Figure 4.16 ATR spectrum of ZnSe/Nujol/PVC system with different thickness of Nujol film.

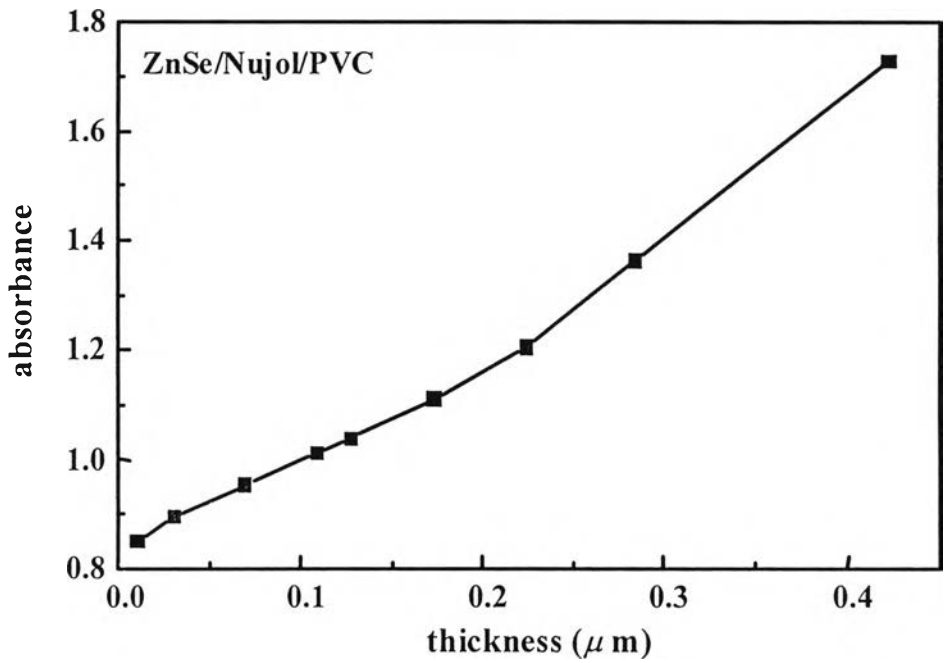

Figure 4.17 Relationship between spectral intensity at 2920 cm^{-1} and thickness of Nujol. The complete spectrum is shown in Figure 14.16.

4.3.2. ATR Spectra of ZnSe/*i*-propanol/PVC System

4.3.2.1. Two-Phase System Spectrum

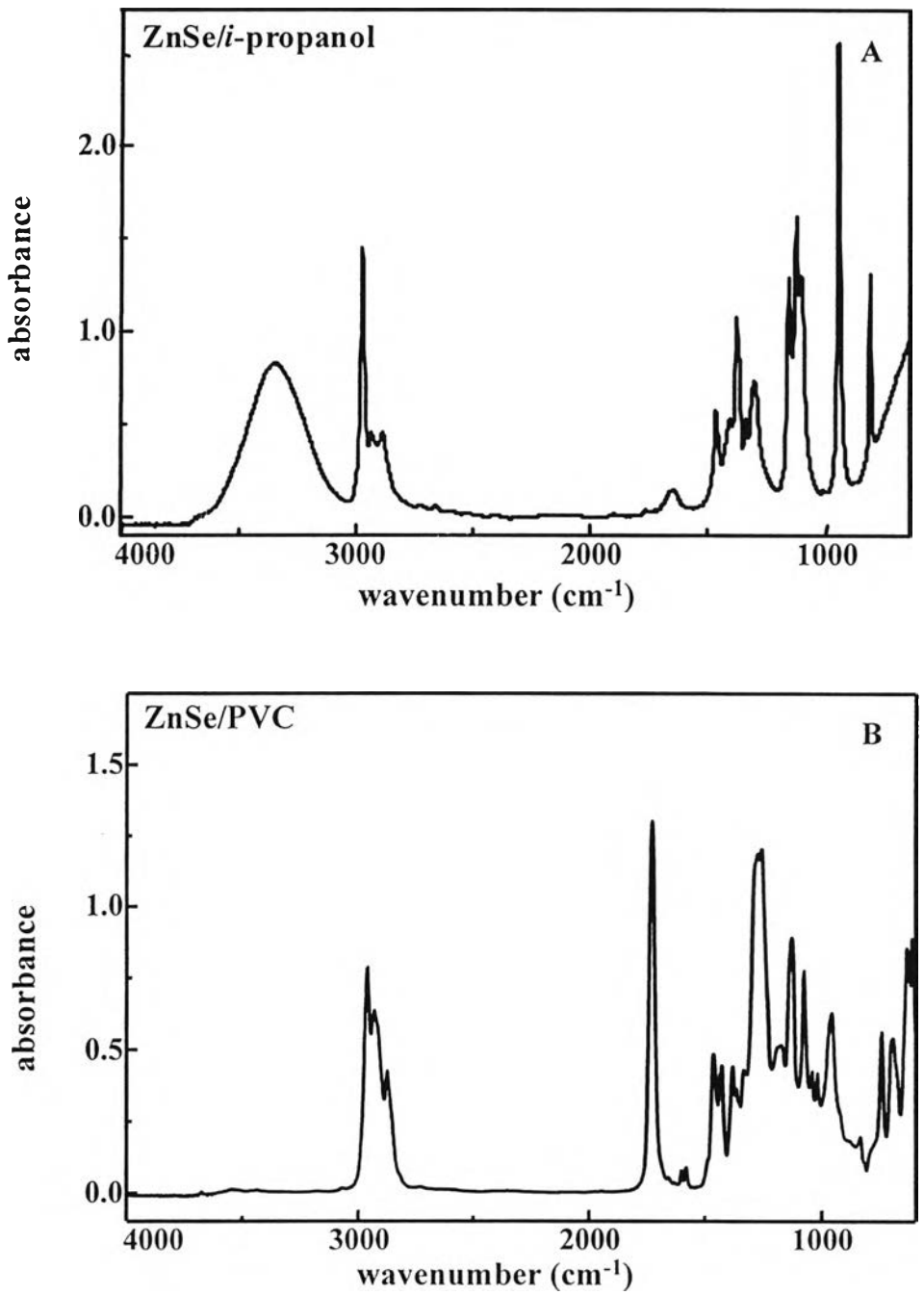

Figure 4.18 ATR spectrum of *i*-propanol and PVC acquired via 45° ZnSe IRE.

4.3.2.2. Three-Phase System Spectrum

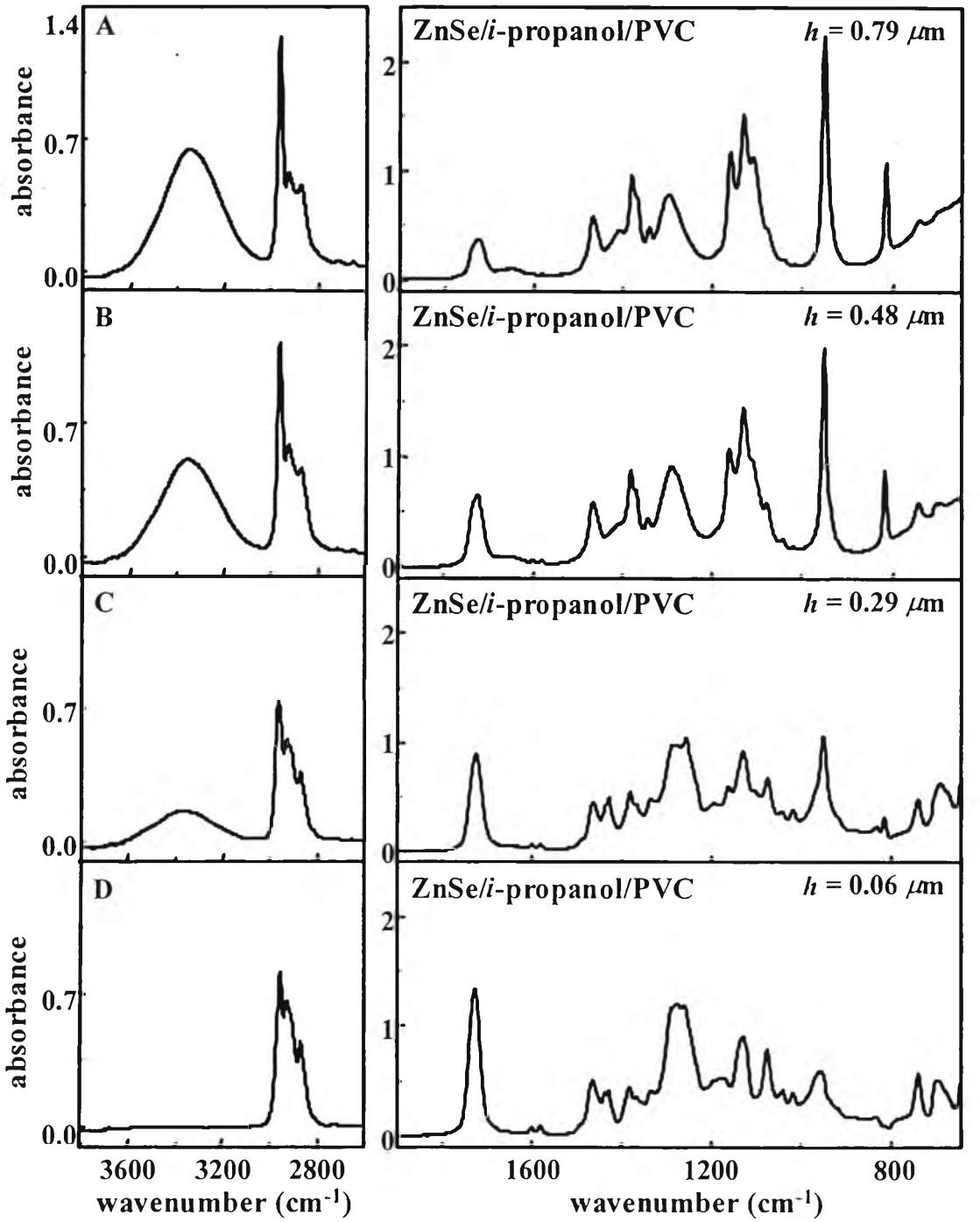

Figure 4.19 ATR spectrum of ZnSe/*i*-propanol/PVC system with different thickness of *i*-propanol film.

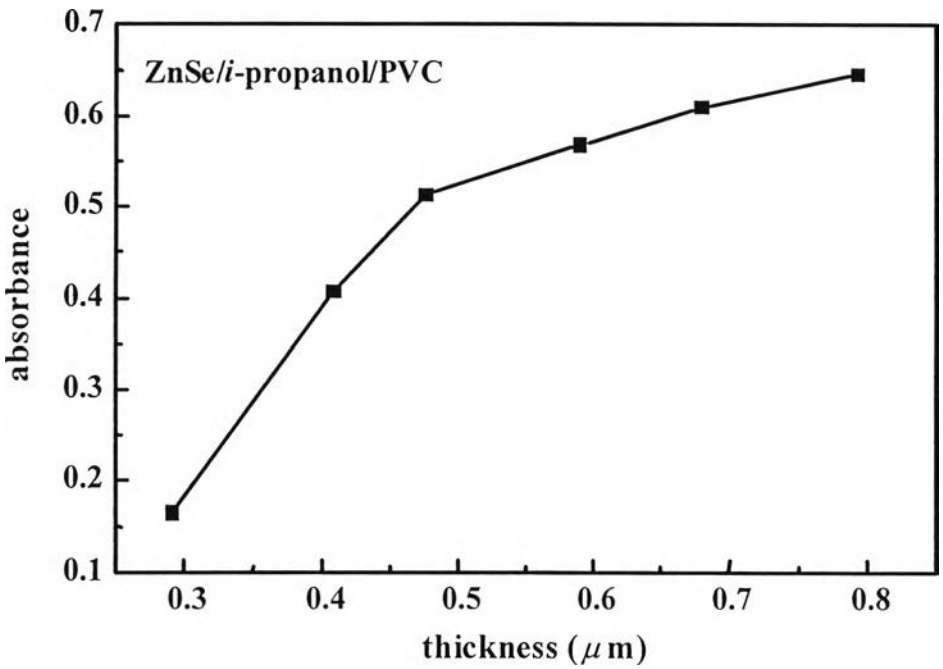

Figure 4.20 Relationship between spectral intensity at 3346 cm^{-1}.and thickness of *i*-propanol. The complete spectrum is shown in Figure 4.19.

4.3.3. ATR Spectra of Ge/Nujol/PVC System

4.3.3.1. Two-Phase System Spectrum

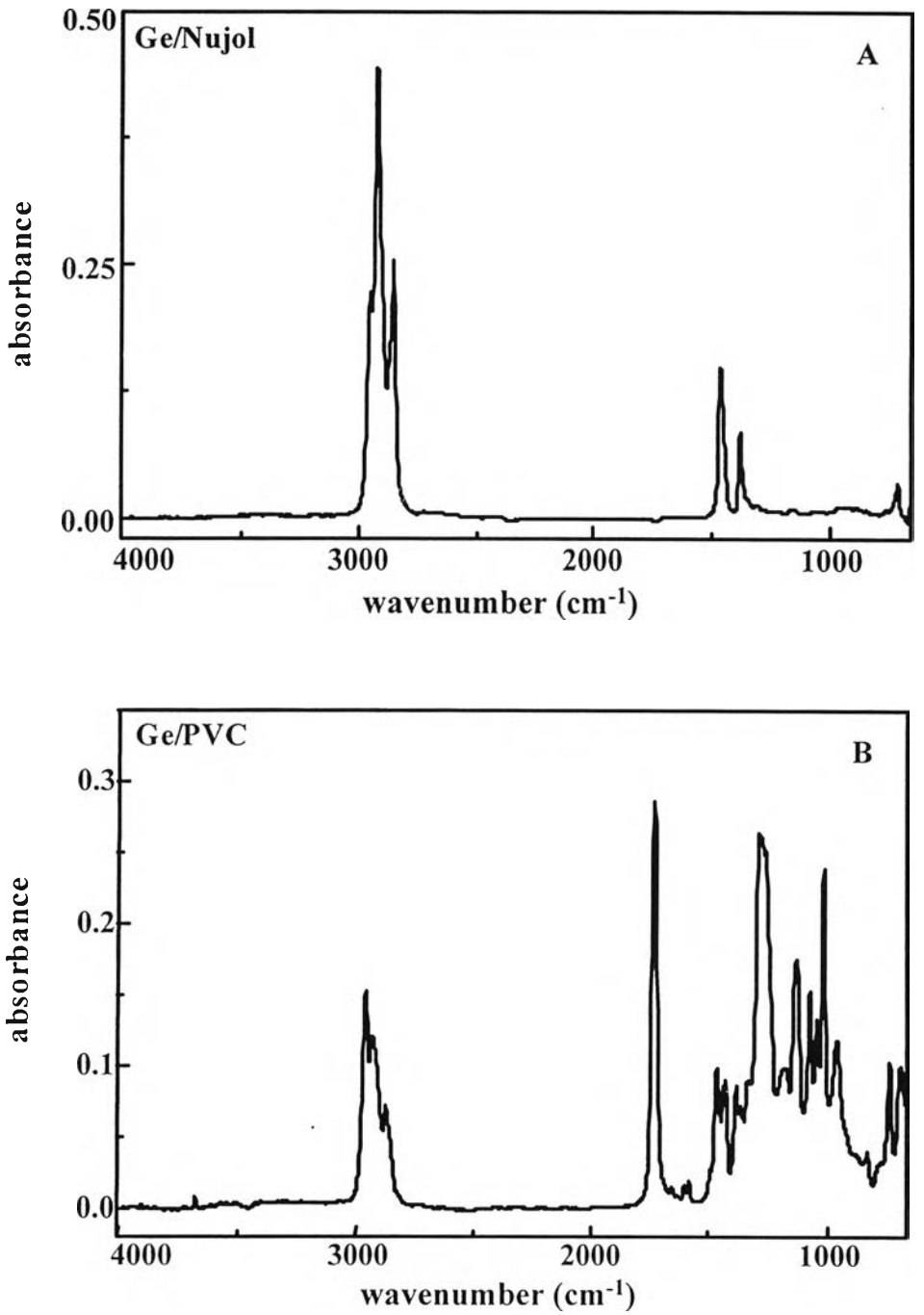

Figure 4.21 ATR spectrum of Nujol and PVC acquired via 45° Ge IRE.

4.3.3.2. Three-Phase System Spectrum

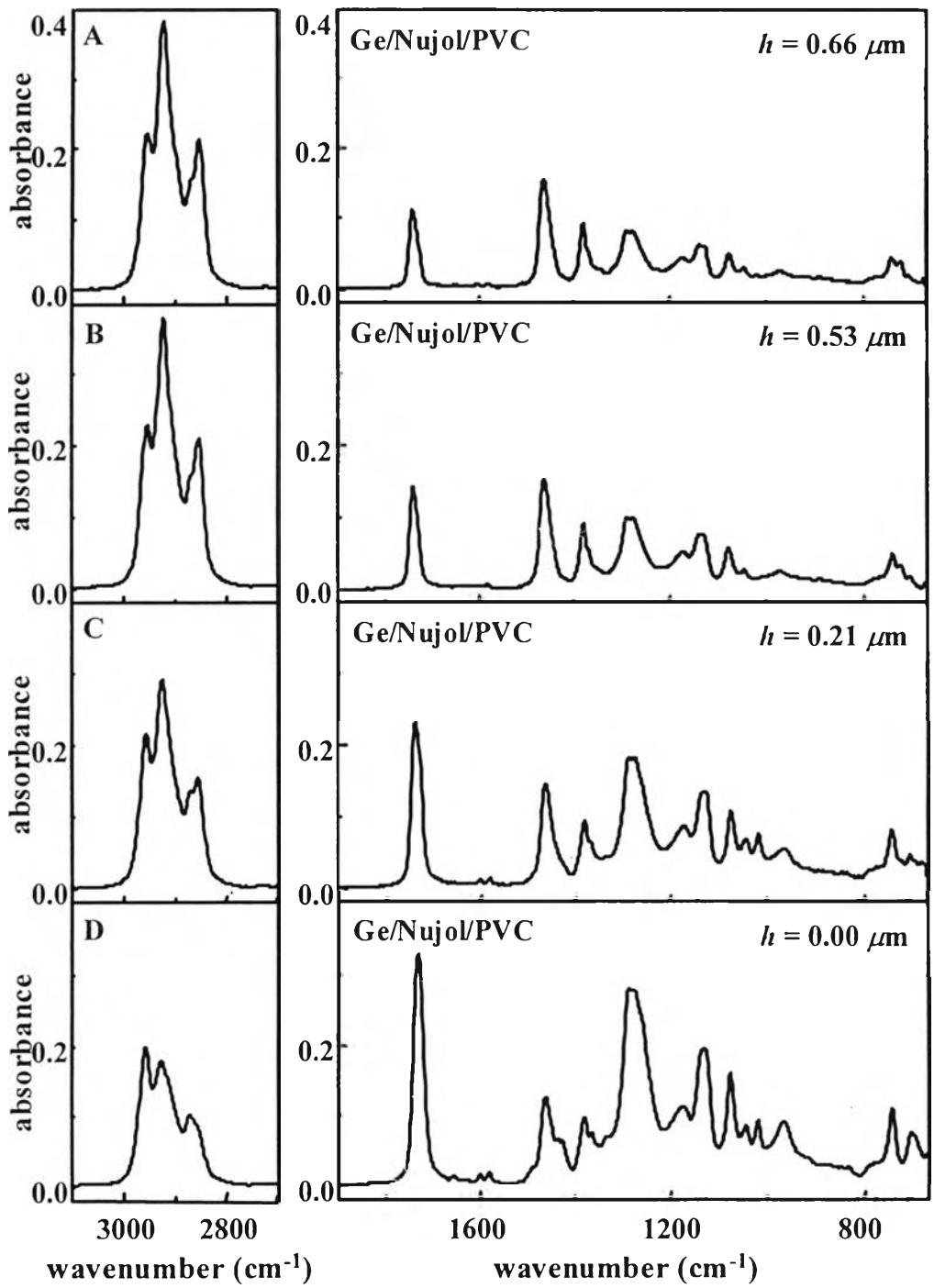

Figure 4.22 ATR spectrum of Ge/Nujol/PVC system with different thickness of Nujol film.

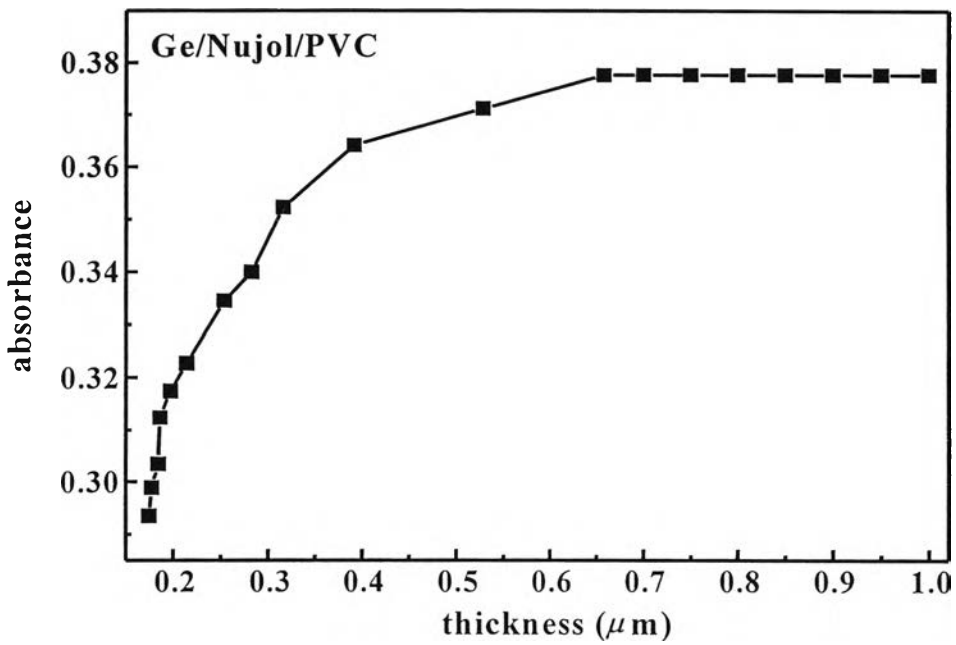

Figure 4.23 Relationship between spectral intensity at 2924 cm^{-1} and thickness of Nujol. The complete spectrum is shown in Figure 4.22.

4.3.4. ATR Spectra of Ge/*i*-propanol/PVC System

4.3.4.1. Two-Phase System Spectrum

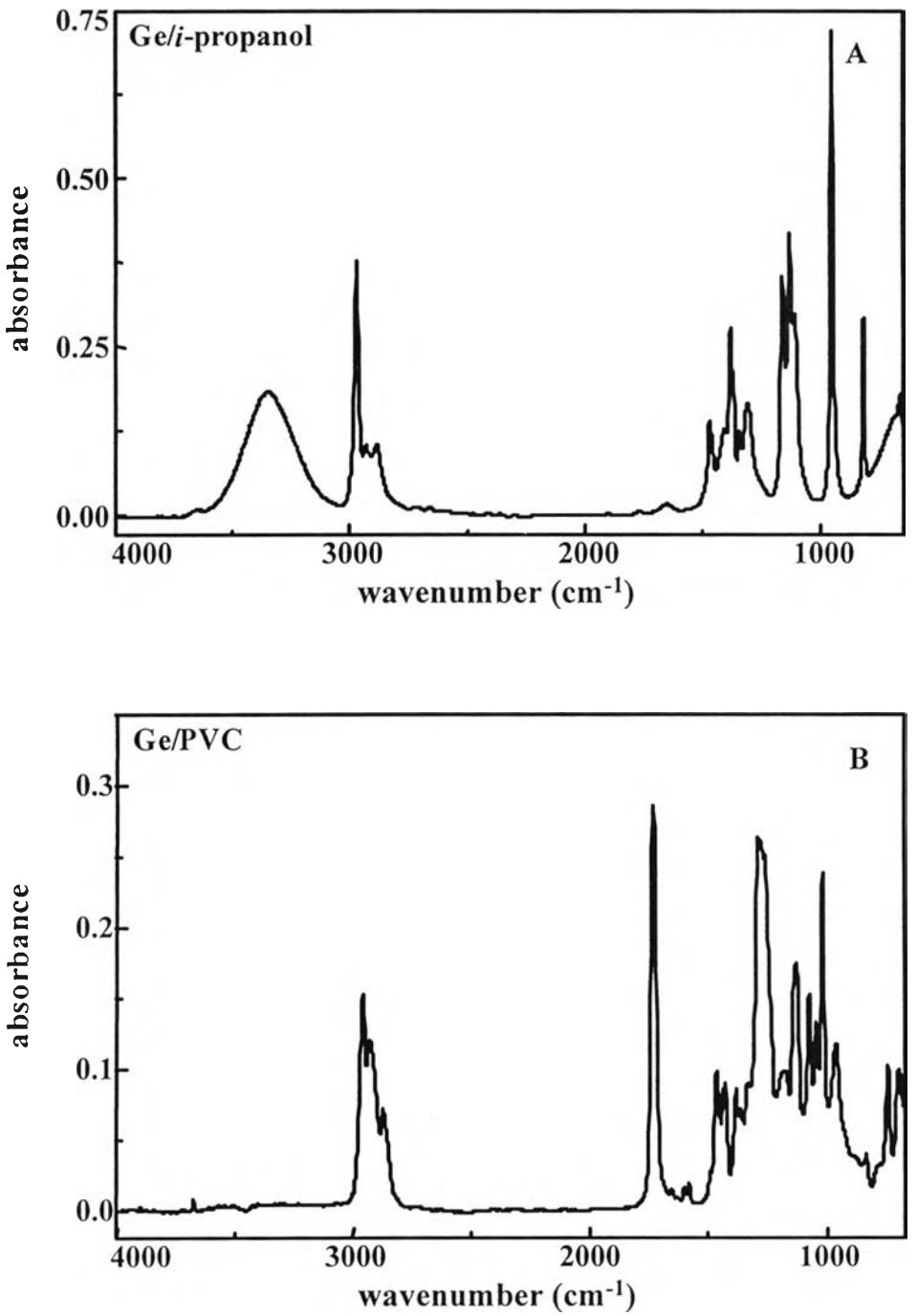

Figure 4.24 ATR spectrum of *i*-propanol and PVC acquired via 45° Ge IRE.

4.3.4.2. Three-Phase System Spectrum

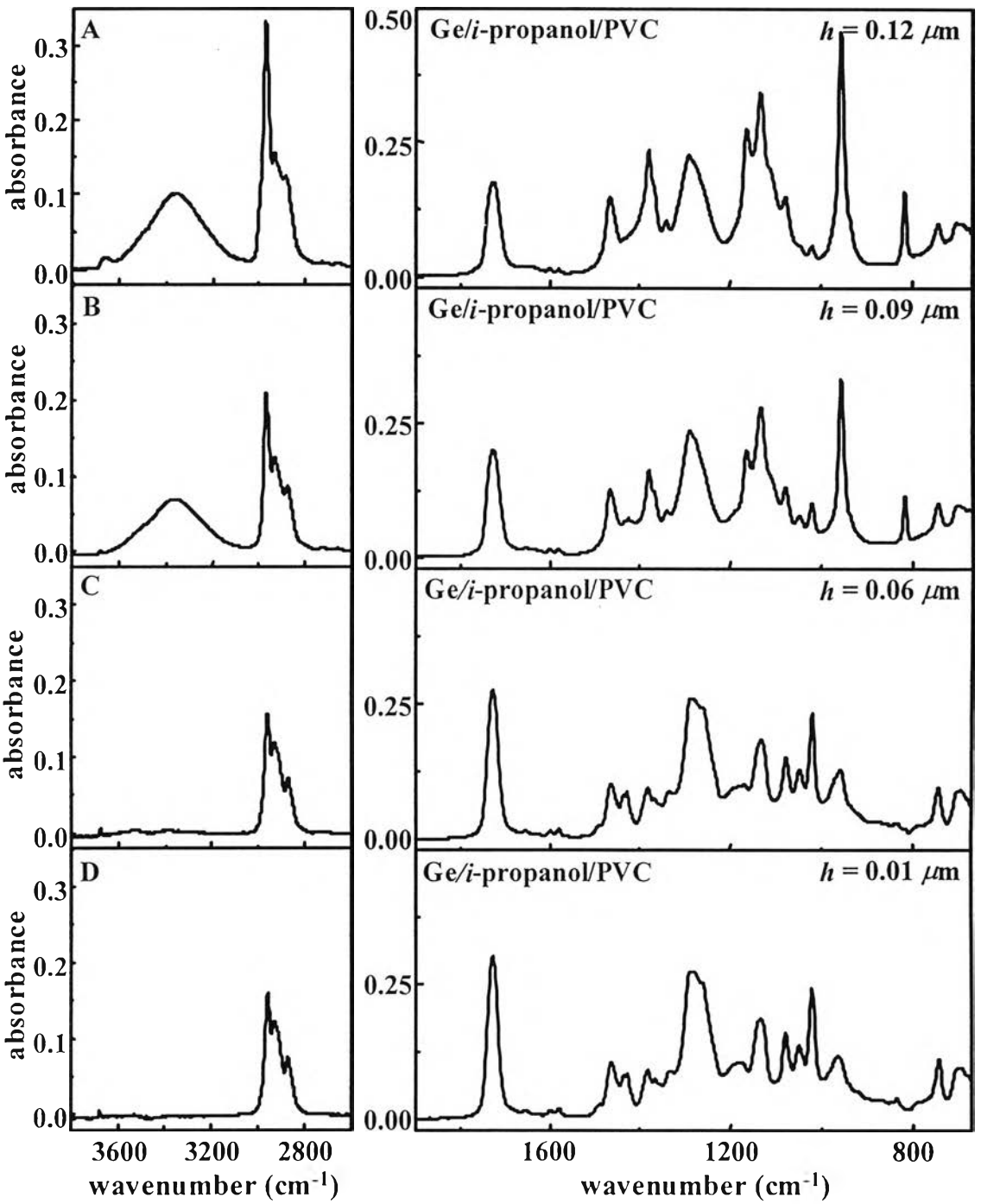

Figure 4.25 ATR spectrum of Ge/*i*-propanol/PVC system with different thickness of *i*-propanol film.

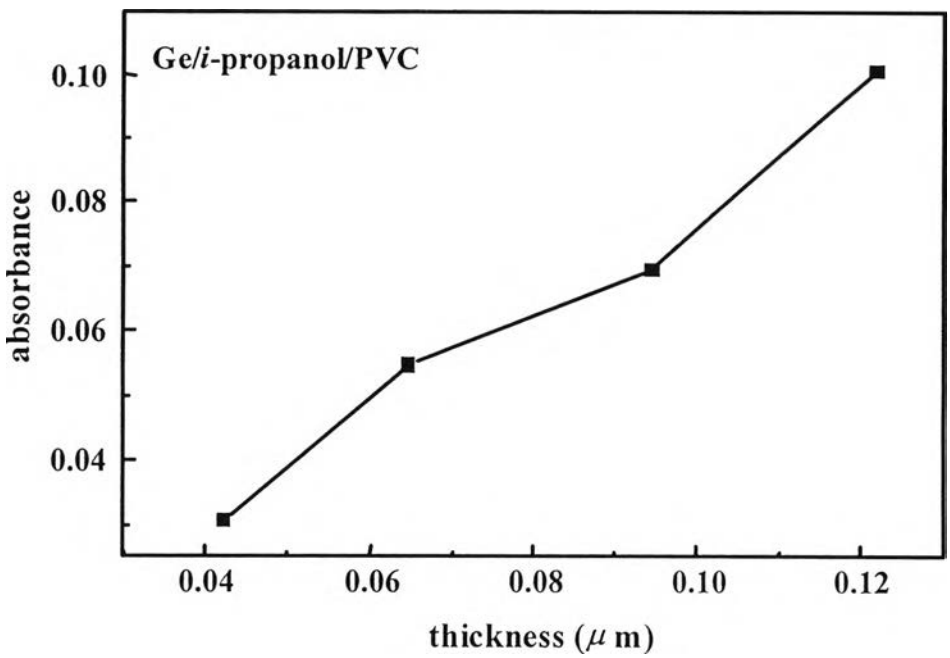

Figure 4.26 Relationship between spectral intensity at 3360 cm^{-1} and thickness of *i*-propanol. The complete spectrum is shown in Figure 4.25.

4.3.5. ATR Spectra of Simulated System

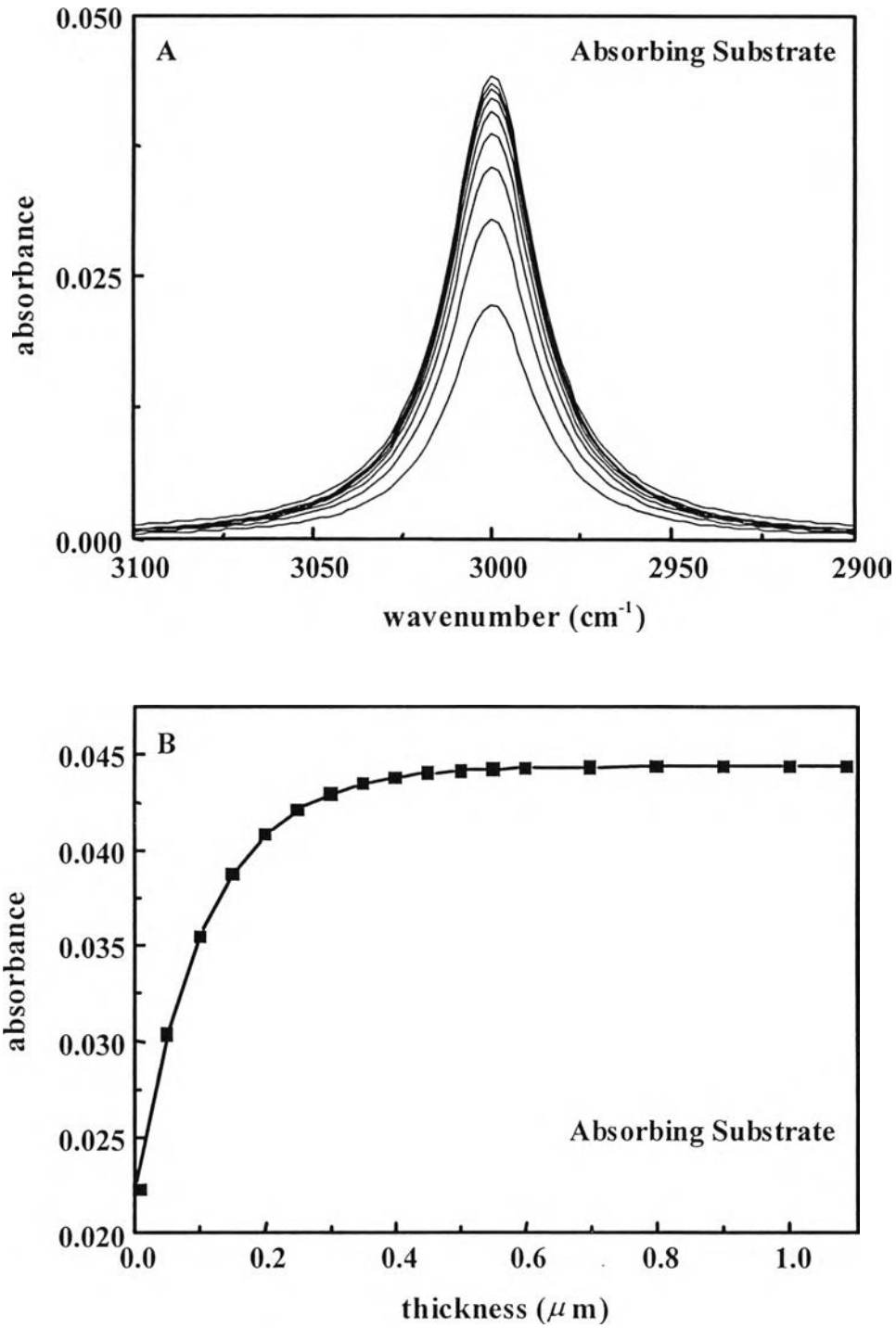

Figure 4.27 Simulated ATR spectrum of film with different thickness (A). Variation of spectral intensity at 3000 cm^{-1} according to film thickness are shown in (B) The simulation parameters are n_{film} = $n_{substrate}$ = 1.5, n_{IRE} = 4.0, and $\theta = 45^{o}$.

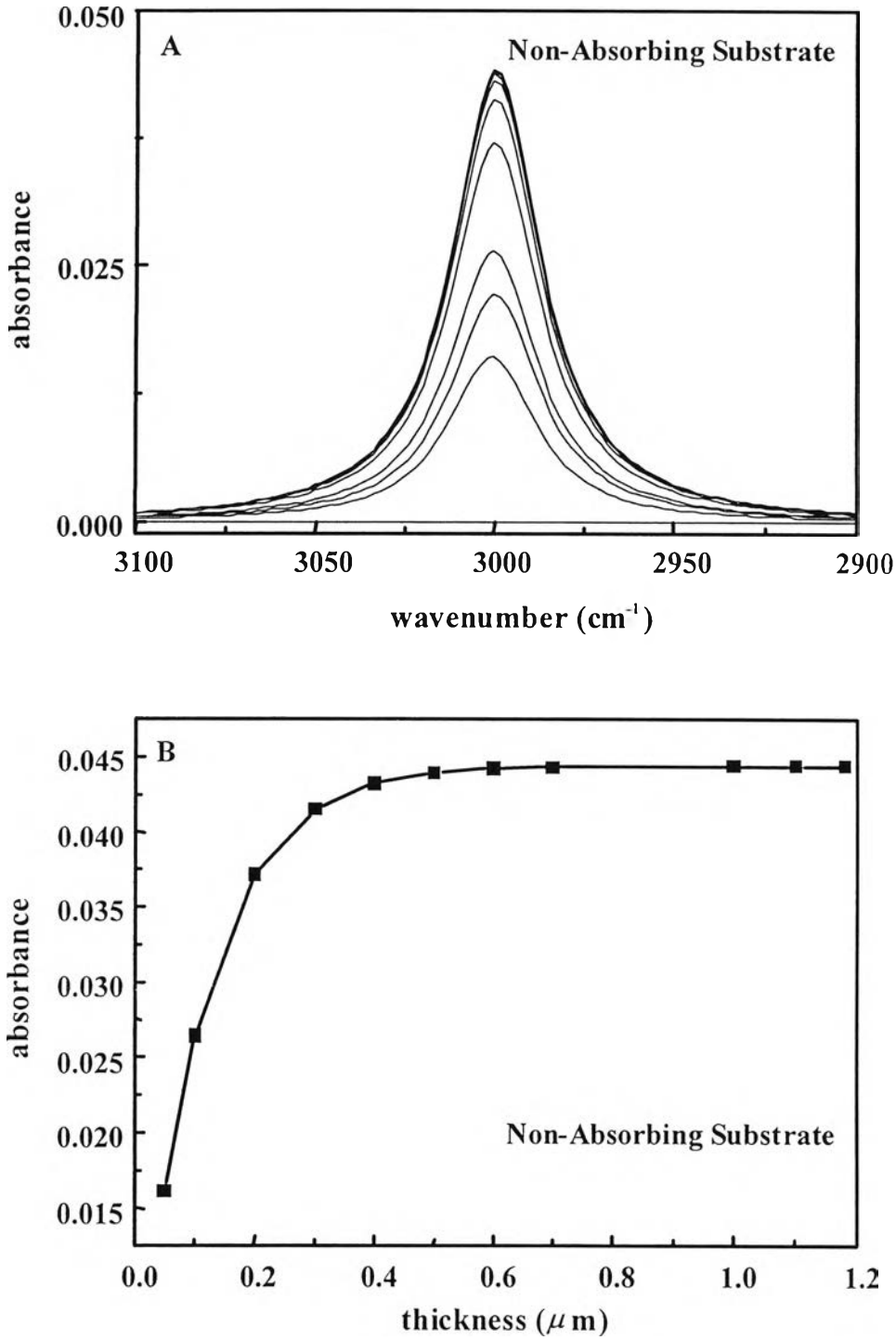

Figure 4.28 Simulated ATR spectrum of film with different thickness (A). Variation of spectral intensity at 3000 cm^{-1} according to film thickness with non-absorbing substrate are shown in (B) The simulation parameters are $n_{film} = n_{substrate} = 1.5$, $n_{IRE} = 4.0$, and $\theta = 45^{o}$.

According to Equations 2.6 and 2.20, an optical contact between IRE and sample is assumed. A small air gap or imperfect contact will largely decrease spectral intensity. Negative error will be obtained from such an effect. In order to avoid the problem related to optical contact, liquid sample is employed instead of solid sample. According to the experimental procedure, thickness of the sample has to be varied. The use of liquid sample will ease the operation since it can be controlled by just squeeze the excess liquid out. Furthermore, this operation will prolong the lifetime of the IRE used in the experiment. The results from this experiment can be readily applied to solid sample or other samples with known refractive index. In fact, the refractive indices of liquid and solid organic materials are the same. The value of 1.5 is normally assumed for the refractive index of organic materials.

However, ATR spectra of solid sample (i.e., PVC sample) were used in the verification of the sampling depth calculated via the proposed equation. Therefore, both two-phase and three-phase ATR spectra are required for the calculation and the verification of sampling depth. The highest ATR spectral intensity of PVC sample obtained from previous optical contact experimental section was assumed as its bulk spectral intensity and was used for calculating the thickness of organic film in three-phase systems.

Two-phase system ATR spectrum of Nujol is shown in Figure 4.15 while its spectral intensities at various wavenumbers are shown in Table 4.2. These spectral intensities will be employed in the calculation of sampling depth. The spectrum was acquired with 45° ZnSe IRE. Since the refractive index of ZnSe and that of the sample is not so much different (i.e., n_{ZnSe} = 2.40 and n_{Nujol} = 1.50). The field strength in the system is quite strong, its decay constant is small (i.e., large $d_p(\theta, \nu)$), and penetrate deeper into the sample. As a result, spectral intensity is quite high according to the relationship given in Equations 2.6 and 2.20. Figure 4.15 B is ATR spectrum of PVC sample acquired via ZnSe IRE without any intermediate layer. Since PVC sample is flexible and has a much better optical contact with the

IRE than PC sample, therefore, it was employed to experimentally verify the proposed equation for sampling depth (i.e., Equation 2.21). In order to calculate the thickness of organic liquid in three-phase system, the spectral intensity of substrate is required. However, the peaks being used for the calculation must be isolated peaks. An overlapped peak should not be employed in order to avoid refractive index dispersion in the system. For the ZnSe/Nujol/PVC system, the absorption band at 1750 cm^{-1} is the most appropriate for thickness calculation since it is an isolated band and is not interfered by absorption bands of Nujol.

Selected ATR spectra of ZnSe/Nujol/PVC system with different thickness of Nujol are shown in Figure 4.16. The thickness of Nujol film was varied by an applied pressure. The thickness is calculated by the relationship given in Equation 2.22. Due to the unique characteristic under total internal reflection condition where the electric field penetrates up to different depths according to wavenumber or frequency being investigated. The greater is the wavenumber or frequency, the shallower the field penetrates into the sample. As a result, thickness of the film calculated from the lower wavenumber can be used to verify the sampling depth at high wavenumber. At the thickness where the sampling depth at high wavenumber is reached, there will be an on-set for spectral intensity changes. The sampling depth at high wavenumber can always be calculated from information at the lower wavenumber using this procedure since the sampling depth at the lower wavenumber is much greater than that of the high wavenumber.

According to the spectra shown in Figure 4.16, the relationship between spectral intensity of Nujol at selected wavenumber (i.e., 2920 cm^{-1}) and its thickness were plotted and are shown in Figure 4.17. It can be seen, from the figure, that the spectral intensity of Nujol decreases continuously as its thickness decreases and there is no region in which the spectral intensity of Nujol is constant (i.e., region beyond the sampling depth). This is because the largest thickness of Nujol film plotted in Figure 4.17 is less than the sampling depth at that wavenumber. The sampling depth of the system (i.e., 45^{o} ZnSe) is greater than 0.4 micrometer.

Next figure is the system of ZnSe/*i*-propanol/PVC. ATR spectrum of *i*-propanol can be seen in Figure 4.18 A. The spectral intensities at various wavenumber of *i*-propanol are listed in Table 4.3 and will be further employed in the calculation of sampling depth. ATR spectrum shown in Figure 4.18 B is two-phase system spectrum of PVC sample acquired via ZnSe IRE. Same as in the previous system, the peak of PVC sample at wavenumber about 1750 cm^{-1} was used to calculate the thickness of *i*-propanol film in three-phase system via Equation 2.18. Selected three-phase system ATR spectra of ZnSe/*i*-propanol/PVC system and the thickness of *i*-propanol film in each spectrum can be seen in Figure 4.19. The sampling depth calculated, in the region of high wavenumber, from *i*-propanol ATR spectrum will be verified with the same procedure as mentioned before. The absorption band of *i*-propanol at wavenumber 3346 cm^{-1} was selected and was monitored as the thickness of *i*-propanol film was varied by an applied pressure. The relationship between spectral intensity of *i*-propanol at the wavenumber and its thickness were plotted and are shown in Figure 4.20. Similar curve as that in the previous system is obtained. As can be seen in Figure 4.20, the spectral intensity of *i*-propanol continuously decreases as the film becomes thinner. The region in which the spectral intensity is constant is not observed. According to this, the sampling depth for this system should be in the region more than 0.8 micrometer.

In this experimental section, in addition to ZnSe IRE, Ge IRE was also used as an incident medium. The Ge IRE used in this experiment has the same physical dimension as that of ZnSe IRE and, therefore, also the same effective number of reflections. The only distinct difference between the two incident media is the refractive index, which is 4.0 for Ge IRE. According to its refractive index, ATR spectral intensity of Nujol acquired via Ge IRE is much lower than that acquired via ZnSe IRE. This is because the electric field at the absorbing/incident media interface in case of Ge IRE has smaller field strength, decays faster, and penetrate to a shallower depth than that of ZnSe IRE. As a result, the spectral intensity of absorbing medium acquired via Ge IRE is so different from that acquired via other lower refractive index IREs. The spectral intensities of Nujol acquired via Ge IRE at various wavenumbers are shown in Table 4.4.

The same substrate used in case of ZnSe IRE were employed in the system using Ge IRE as an incident medium. ATR spectrum of PVC sample is shown in Figure 4.21 B. It can be seen that both the spectral intensities of Nujol and PVC sample are extremely different from those acquired via ZnSe IRE. Like other systems, the thickness of Nujol film was varied by an applied pressure and the peak of PVC sample at wavenumber about 1750 cm^{-1} was used to calculate the thickness of the film and the calculated thickness is shown in each spectrum (see Figure 4.22). The thickness will then be used to verify the sampling depth calculated at high wavenumber like other previous systems. By plotting the spectral intensity of Nujol at wavenumber of interest (i.e., 2924 cm^{-1}) versus its thickness, the relationship shown in Figure 4.23 was obtained. From the curve, unlike in case of ZnSe IRE, the region in which the spectral intensity of Nujol is constant (i.e., the region beyond sampling depth) is observed. This is because ATR is surface sensitive and, thus, any information exists beyond the sampling depth will not contribute in the spectrum. That is why the spectral intensity of Nujol at the region is constant when the thickness of the Nujol film is beyond the sampling depth. The observed constant spectral intensity decreases significantly from its bulk intensity in the region of about 0.6 micrometer and then continuously decreases with the thickness of Nujol film. Therefore, the sampling depth for this system should be in the region of about 0.6 micrometer as well.

The last experimental system, Ge/*i*-propanol/PVC system, is shown in Figure 4.24. ATR spectrum of *i*-propanol acquired via Ge IRE is shown in Figure 4.24 A. The spectral intensity of *i*-propanol at various wavenumbers are shown in Table 4.5. The thickness of *i*-propanol was also varied by an applied pressure as in other systems (see Figure 4.25) and the peak of PVC sample at wavenumber about 1750 cm^{-1} was used in the calculation of *i*-propanol film thickness. The calculated film thickness is shown in each spectrum in Figure 4.25. From the relationship between spectral intensity of *i*-propanol at wavenumber 3360 cm^{-1} and its thickness, the curve shown in Figure 4.26 is obtained. In case of *i*-propanol, unlike in case of Nujol, the variation in its thickness is not fully controllable since it can be evaporated

quite easily and, therefore, the error in the calculation of film thickness occurs and the thickness is not reliable.

Apart from the experimental system using in the verification of the sampling depth calculated via the proposed equation, the simulated systems using Ge IRE as an incident medium were performed. The same procedures treated with experimental systems were employed in the simulated systems as well. The simulated system consists of both two-phase and three-phase systems. The simulated parameters (i.e., optical constants of film, substrate, and incident medium, and the angle of incidence) are the same as experimental parameters. In case of simulated systems, the variation in the thickness of intermediate layer (i.e., organic film in experimental systems) is perfectly controllable. The simulated ATR spectra in case of substrate is absorbing and non-absorbing media at selected wavenumber (i.e., wavenumber 3000 cm^{-1}) are shown in Figures 4.27 A and 4.28 A, respectively and the bulk spectral intensity of simulated intermediate layer at wavenumber 3000 cm^{-1} is shown in Table 4.6. From Figures 4.27 A and 4.28 A, the spectral intensities of simulated intermediate film were plotted against film thickness and their relationships are shown in Figure 4.27 B and 4.28 B for absorbing substrate and non-absorbing substrate, respectively. From these curves, similar results as in cases of experimental systems are observed. In the region of high wavenumber the spectral intensity of simulated film is constant since it is the region beyond the sampling depth and, thus, no contribution from that region involved in the spectrum. The regions of the sampling depth at wavenumber 3000 cm^{-1}, as can be seen from the curves in Figures 4.27 B and 4.28 B, are about 0.40 micrometer.

4.3.6. Sampling Depth

In order to determine the sampling depth in ATR FT-IR spectroscopy, optical contact between sample and the IRE is required. Liquid sample such as Nujol and *i*-propanol are employed as an intermediate layer in three-phase system. It spectral intensity is employed for the calculation of the sampling depth via the proposed equation instead of that of substrate or solid sample. This is because liquid sample always has optical contact with the IRE and, therefore, should give the most reliable result. Furthermore, liquid sample can be varied in thickness conveniently. This leads to the verifiable of the sampling depth calculated via the proposed equation as described before. On a contrary, in case of solid samples, it is quite difficult and more complicate to vary the thickness of samples since solid samples have to be prepared in various different uniform thicknesses. Moreover, the experimental procedure will take much more time for the replacement of the sample by another one with different thickness.

The spectral intensity of Nujol and *i*-propanol shown in two-phase system spectra acquired via both ZnSe IRE and Ge IRE were employed for the calculation of sampling depth at various wavenumbers. Average noise level in each spectrum was also introduced into the calculations as can be seen in Equation 2.21.

The sampling depths calculated from each system are shown in the following tables.

4.3.6.1. **ZnSe/Nujol System** (ZnSe, $n = 2.4$)

Table 4.2 Sampling depth and penetration depth calculated from ZnSe/Nujol system by using the spectral intensity of Nujol at various wavenumbers and the average noise level in the spectrum.

wavenumber (cm^{-1})	**spectral intensity**	**penetration depth** (d_p, μm)	**sampling depth** (μm)
2953.01	0.129	0.6790	1.7808
2920.22	**0.252**	**0.6867**	**2.0309**
2852.71	0.177	0.7029	1.9547
1460.11	0.103	1.3733	3.4473
1377.17	0.064	1.4560	3.3084
721.37	0.030	2.7797	5.2632

Noise Level: 3.4×10^{-4}

4.3.6.2. **ZnSe/*i*-propanol System** (ZnSe, n = 2.4)

Table 4.3 Sampling depth and penetration depth calculated from ZnSe/*i*-propanol system by using the spectral intensity of *i*-propanol at various wavenumbers and the noise level in the spectrum.

wavenumber (cm^{-1})	**spectral intensity**	**penetration depth (d_p, μm)**	**sampling depth (μm)**
3346.49	**0.111**	**0.5992**	**1.4340**
2970.37	0.194	0.6751	1.8041
2933.72	0.061	0.6835	1.4312
2883.57	0.061	0.6954	1.4561
1465.90	0.078	1.3679	3.0324
1379.10	0.144	1.4540	3.6689
1305.80	0.098	1.5356	3.5794
1159.21	0.173	1.7298	4.5236
1128.35	0.217	1.7771	4.8486
948.97	0.345	2.1130	6.2549
815.89	0.176	2.4577	6.4482

Noise Level : 4.63×10^{-4}

4.3.6.3. **Ge/Nujol System** (Ge, n = 4.0)

Table 4.4 Sampling depth and penetration depth calculated from Ge/Nujol system by using the spectral intensity of Nujol at various wavenumbers and the noise level in the spectrum.

wavenumber (cm^{-1})	**spectral intensity**	**penetration depth (d_p, μm)**	**sampling depth (μm)**
2953.01	0.030	0.2248	0.4911
2924.08	**0.060**	**0.2270**	**0.5745**
2854.64	0.034	0.2325	0.5224
1462.04	0.020	0.4540	0.8997
1377.17	0.012	0.4820	0.8321
721.37	0.005	0.9201	1.1401

Noise Level : 1.9×10^{-4}

4.3.6.4. Ge/*i*-propanol System (Ge, n = 4.0)

Table 4.5 Sampling depth and penetration depth calculated from Ge/*i*-propanol system by using the spectral intensity of *i*-propanol at various frequencies and the noise level in the spectrum.

wavenumber (cm^{-1})	**spectral intensity**	**penetration depth (d_p, μm)**	**sampling depth (μm)**
3346.49	**0.184**	**0.1983**	**0.4273**
2970.37	0.377	0.2235	0.5613
2931.80	0.104	0.2264	0.4222
2885.50	0.107	0.2300	0.4289
1467.82	0.140	0.4522	0.9123
1379.10	0.279	0.4813	1.1314
1307.73	0.167	0.5075	1.0611
1161.14	0.355	0.5716	1.4181
1128.35	0.417	0.5882	1.5046
950.90	0.720	0.6980	1.9772
815.89	0.291	0.8135	1.9338

Noise Level : 1.68×10^{-4}

4.3.6.5. Simulated System (Ge, n = 4.0)

Table 4.6 Sampling depth and penetration depth calculated from simulated system at wavenumber 3000 cm^{-1}.

wavenumber (cm^{-1})	spectral intensity	penetration depth (d_p, μm)	sampling depth (μm)
3000.00	0.044	0.2212	0.3429

Noise Level : 1.00×10^{-3}

The sampling depth and also the penetration depth calculated at various wavenumbers of ATR spectra of Nujol and *i*-propanol are shown in Tables 4.2 to 4.5 and those calculated from simulated system are shown in Table 4.6. Since Equation 2.15, which is used in the calculation of sampling depth, is assumed under single reflection condition, thus, all of the spectral intensities employed in the calculation, obtained from the experiment using multiple reflection IRE, were divided by the effective number of reflections in the IRE before being employed in the calculation (i.e., ZnSe and Ge IREs have effective number of reflections 7.45). The spectral intensities shown in all tables, therefore, represent the spectral intensity of single reflection. The noise level used in the calculation is the average value determined from the non-absorbing region in the spectrum.

It can be seen, from all tables, that the penetration depth ,$d_p(\theta, \nu)$, varies as a function of wavenumber. This is the unique characteristic under total internal reflection condition. The penetration depth at each wavenumber was used in the determination of sampling depth at that particular wavenumber. The sampling depth, on the other hand, varies not only as a function of wavenumber but also the spectral intensity and the noise level in the observed spectrum. Therefore, unlike the penetration depth, the sampling depth at higher wavenumber may be larger than that at lower wavenumber depending on the spectral intensity at that wavenumber.

According to Figures 4.17, 4.20, and 4.26, as described before, the thickness of organic film at which its spectral intensity is constant was not observed. As a result, these relationships can not be employed in the verification of the calculated sampling depth. However, according to Figure 4.23, in case of Ge/Nujol/PVC system, which is the most appropriate system (i.e., small absorption condition and controllable film thickness), the relationship between the spectral intensity of Nujol and its thickness can be used to verify the calculated sampling depth. As can be seen, from the curves shown in Figure 4.23, that the spectral intensity of Nujol is constant when the thickness is greater than 0.60 micrometer. Spectral intensity decreases continuously as the thickness of Nujol film becomes smaller. It is the region in which the spectral intensity decreases significantly from its bulk intensity that the sampling depth has been reached. From Table 4.4, the calculated sampling depth at wavenumber 2924 cm^{-1} is 0.575 micrometer. It can be seen that the sampling depth calculated via the proposed equation agree quite well with the experimental result.

In case of simulated system the wavenumber used in the simulation is 3000 cm^{-1} of which the calculated sampling depth is 0.343 micrometer. It can be seen that the sampling depth calculated via the proposed equation agree quite well with the simulated results. By comparing the simulated results to Figures 4.27 B and 4.28 B, the thickness of liquid film at which the film spectral intensities start decreasing are about 0.4 micrometer.